Spring 1-1-2018

The Role of Magnesium in the Acid Degradation of Metakaolin-Based Alkali-Activated Cements

Zoey Marie Craun
University of Colorado at Boulder, zoeycraun@gmail.com

Recommended Citation

Craun, Zoey Marie, "The Role of Magnesium in the Acid Degradation of Metakaolin-Based Alkali-Activated Cements" (2018). *Civil Engineering Graduate Theses & Dissertations*. 352.
https://scholar.colorado.edu/cven_gradetds/352

THE ROLE OF MAGNESIUM IN THE ACID DEGRADATION OF METAKAOLIN-BASED ALKALI-ACTIVATED CEMENTS

by:

ZOEY MARIE CRAUN

B.S. University of Colorado Boulder, 2017

A thesis submitted to the
Faculty of the Graduate School of the
University of Colorado in partial fulfillment
of the requirement for the degree of
Master of Science
Architectural Engineering
2018

This thesis entitled:
The Role of Magnesium in the Acid Degradation of Alkali-Activated Cements

written by Zoey Marie Craun

has been approved
for the Department of Civil, Environmental, and Architectural Engineering

____

Prof. Wil V. Srubar III

____

Prof. Mija H. Hubler

____

Prof. JoAnn Silverstein

Date________________

The final copy of this thesis has been examined by the signatories, and we find that both the content and the form meet acceptable presentation standards of scholarly work in the above mentioned discipline.

Craun, Zoey Marie (M.S., Architectural Engineering)

The Role of Magnesium in the Acid Degradation of Alkali-Activated Cements

Thesis directed by Assistant Professor Wil V. Srubar III

Microbial-induced concrete corrosion (MICC) of ordinary portland cement (OPC) concrete sewers is a major infrastructure challenge in the United States (US). Many US municipalities make significant annual financial investments every year for the continual maintenance and replacement of sewer lines—the majority of which have exceeded their design life—to keep them operational. Utilization of alkali-activated cement (AAC), a novel cementitious material that is an alternative to OPC, in sewer applications presents an opportunity to increase the durability of concrete sewer systems. AACs are chemically activated binders made from waste (e.g., fly ash, slag) and natural (e.g., metakaolin) aluminosilicate precursors that often have variable elemental compositions. While in some cases AAC concrete has been shown to exhibit higher acid resistance than its OPC counterparts, the actual mechanism of acid degradation in AACs is not yet fully understood, in part, due to the complex and variable chemistry of the aluminosilicate precursors. This study systematically evaluates the role of a magnesium mineral addition in the form of brucite on the acid degradation of metakaolin-based AACs. The effects of (1) silica content, (2) sodium content, and (3) magnesium mineral addition on the structure (i.e., mineralogy) and properties (i.e., porosity, acid resistance) of AACs are investigated herein. After synthesis, AAC samples were exposed to sulfuric acid solutions with a pH of 2.00 ± 0.05 and allowed to reach equilibrium (defined as a change in pH of less than 0.01 per 4 hours). In order to determine the effect of magnesium mineral addition on the acid durability of AACs, porosity measurements were taken before and after acid exposure. Mineralogy of the samples was determined using X-ray diffraction. Leaching data were collected after the samples reached equilibrium. In addition, this work utilizes a central composite design to develop response surfaces for leaching and porosity to better understand and predict the effect of different alkali and silica contents and mineral additions. Finally, elemental maps produced using electron microprobe analysis (EMPA) were used to visualize the acid corrosion front and diffusion of magnesium ions throughout the AAC samples. These maps are also used to confirm current understanding of how calcium-free AACs respond to exposure to sulfuric acid. Results substantiate that adding unreacted magnesium mineral content to the AACs improves the acid resistance of the material by improving the stability of the aluminosilicate structure as evidenced by a reduction in the amount of leached silicon and aluminum during acid exposure.

ACKNOWLEDGMENTS

I would like to start off by thanking my advisor, Dr. Wil V. Srubar III, for offering his advice and expertise on this thesis as well as other projects I have been involved in as a part of the SIMLab over the past 3 years. I would also like to give special thanks to my mentor in the lab, Juan Pablo Gevaudan, for training me and being available to offer assistance and advice whenever I needed it. Finally, I would like to thank my committee members, Dr. Mija H. Hubler and Dr. JoAnn Silverstein, for their time, consideration, and insight on this work.

Special appreciation also goes out to all of the members of the SIMLab for their help and advice in the lab and for constantly inspiring me to be a better scientist and engineer. I also appreciate the support provided by the National Science Foundation for this project.

Last but not least, I would like to thank my parents, John and Kari Craun, for supporting me throughout my undergraduate and graduate careers as well as in life in general.

CONTENTS

LIST OF TABLES

LIST OF FIGURES

CHAPTER 1 INTRODUCTION

The maintenance and replacement of sewer systems within the United States (US) requires significant financial investment. In the US alone, public sewer lines total over 800,000 miles in length with an additional 500,000 miles of private lateral sewer lines and many of those miles will need to be replaced or rehabilitated in the near future [1]. The results from a 1998 survey of 42 municipal sewer systems found that the average age of the pipes within their systems was around 33 years old. This finding is significant because the average sewer pipe is only expected to last around 50 years (CBO, 2002). Because much of the wastewater infrastructure in the U.S. is reaching the end of its design life, significant investment must be made in the maintenance and replacement of these systems to keep them operational. In the EPA's 2012 Clean Watersheds Needs Survey, the documented need for wastewater pipe repair and new pipe was estimated to be $95.7 billion—a number that will only continue to grow [3].

One of the major contributors to the deterioration of sewer systems is microbial-induced concrete corrosion (MICC). Biogenic sulfuric acid is produced in sewers as a result of the oxidation of hydrogen sulfide gas by bacteria [4]. This process leads to MICC when the biogenic sulfuric acid reacts with calcium-containing components in the cured concrete to form the corrosion products gypsum and ettringite [4] [5]. The acidic corrosion of concrete structures is a major cause of deterioration, and corrosion due to sulfuric acid is the most common form of this mechanism [6]. Previous studies on concrete in wastewater environments have shown that the rate of corrosion due to the exposure to biogenic sulfuric acid of ordinary portland cement (OPC) can range from 3.7 to 7.7 mm per year [7]. Higher temperatures have been shown to enhance the processes of acidification at the surface of the concrete, potentially resulting from an increase in the rate of the chemical and biological reaction [4]. In the future, climate change and resulting elevated temperatures can be expected to exacerbate the issue.

Novel cementitious materials, such as alkali-activated cements (AACs), are an alternative to OPC and offer a potential opportunity to increase the durability of concrete sewer systems. AACs are cements that gain their strength by way of a chemical reaction between a source of alkali (soluble base activator such as a sodium silicate or sodium hydroxide solution) and aluminate-rich materials (such as fly ash, slag, or metakaolin). Concrete made with OPC is highly vulnerable to acidic media because of its high calcium content and because its hydration products are not stable at low pH. Previous studies have shown that AACs are more resistant to acid attack than OPC [8], [9]. Two of the main factors contributing to AACs potential for improved acid resistance and durability include a reduced amount of calcium hydroxide in comparison to OPC as well as the opportunity to tailor mix designs with different combinations of aluminosilicates and alkali-activating sources to best suit the environmental conditions to which the material will be exposed [10]. In addition to increasing durability, AACs can have reduced carbon footprints compared to OPC, even after factors related to the production and transportation of the alkali activator are taken into consideration [11]. While AACs show promising characteristics, before they can be implemented on a wider scale as a mainstream material, further testing needs to be done to evaluate their performance under different environmental conditions to ensure a more complete understanding of their long-term durability.

This thesis presents a study evaluating the acid degradation response of a calcium-free AAC with a magnesium-based mineral addition, formulated according to a central composite design to allow for statistical analysis. In Chapter 2, the current literature regarding the reaction mechanisms and hydration products of AACs and OPC is discussed. Following this chapter is a breakdown of the deterioration mechanisms of AACs and OPC when exposed to acidic environments as they are currently understood. The final part of the literature review examines specific factors affecting the acid resistance of AACs and opportunities to improve the long-term durability of these materials.

Chapter 3 of this thesis discusses the specific materials and methods used in this study, which includes a description of the central composite mixture design as well as the specific formulations of the AAC evaluated in this study, including the amounts of metakaolin precursor and combined sodium hydroxide and sodium silicate activating solution. The mixing procedure and curing conditions are noted as well. In addition, detailed descriptions of the methodologies used to evaluate the acid resistance of the AACs are provided. These methods include: bulk permeable porosity, dimensional shrinkage, elemental leaching, x-ray diffraction, and electron microprobe analysis. In Chapter 4, the results regarding the performance of these

AAC formulations in a sulfuric acid solution are presented. The response surface models developed using the data collected are also shown in Chapter 4 and trends in the data are identified. Chapter 5 goes into more detail on the findings of the study and offers further explanation behind the results of the study and its contribution to the current literature on the design of calcium-free AACs for improved acid resistance and long-term durability. Chapter 6 provides a summary of the major findings of this study, its limitations, and the potential for future work in the area of tailoring the design of AACs to respond to specific environments.

CHAPTER 2 LITERATURE REVIEW

2.1 OVERVIEW OF AACS

AACs are cementitious materials that are made by reacting a primary aluminosilicate source, which could be a natural material, an industrial by-product, or a combination, with an alkali activating solution. Some of the most common aluminosilicate materials include ground granulated blast furnace slag (GGBFS), fly ash, and metakaolin. GGBFS is formed when slag, a by-product of the iron production process, is rapidly chilled, producing a glassy, granular material. Metakaolin is a calcined form of the clay kaolinite. Alkali activators, such as sodium hydroxide (NaOH) or sodium silicate (NaSi), are mixed with the aluminosilicate source, causing it to set and harden [12].

One of the benefits to using AACs is the ability to design the material to alter its specific microstructural characteristics. In this way, due to the potential for improved durability, materials can be tailored to address specific infrastructure applications. However, because this is a novel class of materials with many different factors resulting in different properties, it is important to continue developing a comprehensive understanding of how different mix designs result in the formation of different reaction products and structures. With this knowledge, the formulations of AACs can be better designed to resistance specific degradation mechanisms such as microbial-induced concrete corrosion (MICC).

2.2 REACTION MECHANISMS AND HYDRATION PRODUCTS

The differing reaction mechanisms and resulting reaction products formed in the activation of OPC, AACs with high-calcium content, and AACs with low-calcium content are key factors in understanding the overall durability of the material, as well as the more specific performance of the material when exposed to acid. This section discusses the hydration mechanisms of OPC and activation mechanisms of high-calcium and low-calcium AACs, as well as their reactions products.

2.2.1 OPC

There are four main mineral components in OPC: calcium silicate materials, including alite (C_3S) and belite (C_2S), as well as calcium aluminate (C_3A) and calcium ferrite (C_4AF) minerals. After water is added to the cement, several chemical reactions immediately take place. The most significant reaction in terms of the strength development of cement is the hydration of the calcium silicates to form calcium silicate hydrate, or C-S-H, gel with a high Ca:Si ratio. Calcium hydroxide is also produced in this reaction. C_3A and water, along with added gypsum, react to form ettringite. Additional C_3A reacts with the ettringite formed to produce monosulfoaluminate.

The C-S-H gel that forms can be described as having a tobermorite-like structure composed of Ca^{2+} ions interlayered between dreierketten chains of silicate tetrahedra. A visualization of this structure created by [12] is shown in **Figure 1**.

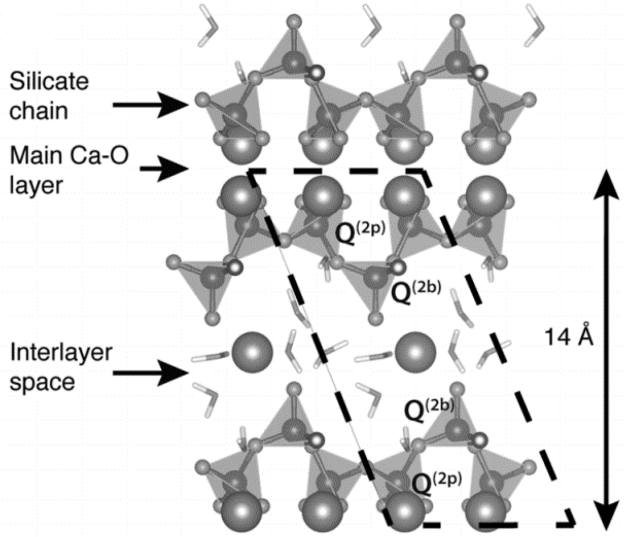

Figure 1. Structure of polymer chains in C-S-H [13]

2.2.2 High-calcium AACs

When high-calcium AACs are created using GGBFS, the main hydration product formed is a C-A-S-H-type gel with a low Ca:Si ratio. In instances where some of the Ca^{2+} is replaced by Na^{+}, the resulting gel formed is described as C-(N)-A-S-H. According to [14], the structural development of these materials is mainly governed by four mechanisms. The first mechanism involves the dissolution of the slag precursor particles. Dissolution is followed by nucleation and growth of the initial solid phases. After these phases are formed, interactions and mechanical binding occurs at their boundaries. The structure continues to develop through an ongoing reaction via dynamic chemical equilibria and diffusion of reactive species through the reaction products formed at advanced times of curing [15].

One of the main differences between the C-S-H and C-A-S-H gels is that the low Ca:Si ratio and high aluminum content present in the latter allow for the possibility of cross-linking between dreierketten chains in the tobermorite-like units as depicted in **Figure 2**.

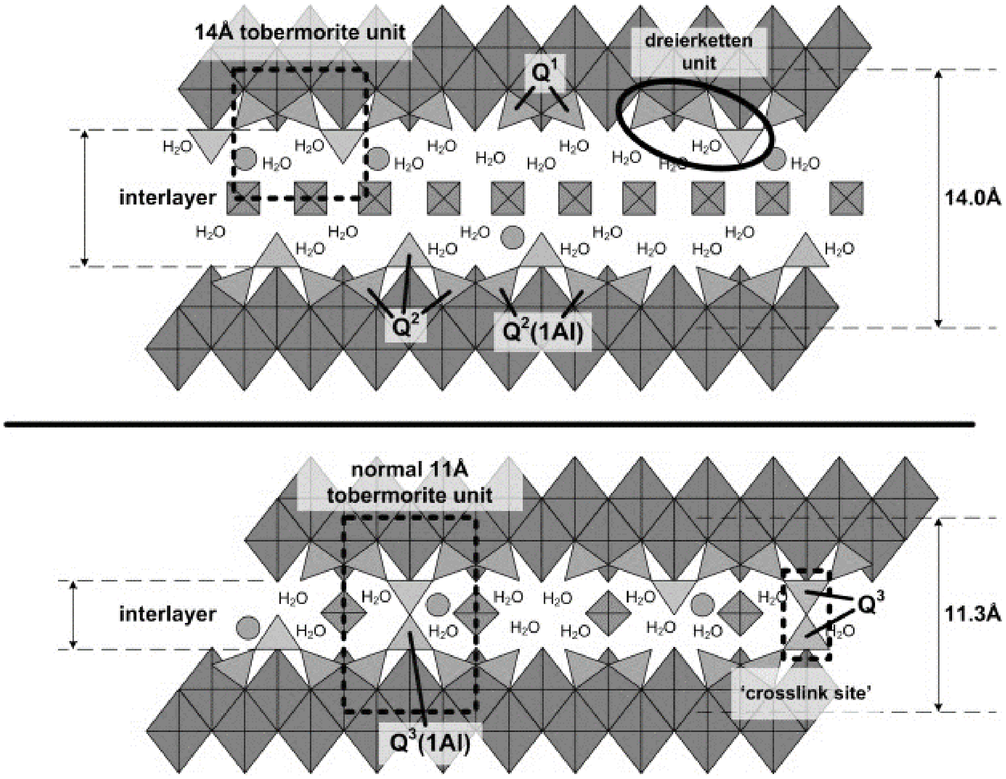

Figure 2. Structure of C-A-S-H gel showing the possible crosslink site [9]

2.2.3 Low-calcium AACs

When low-calcium or calcium-free AACs are created using Type F fly ash or metakaolin as the primary raw material, the result is a high-silica, high-alumina, low-calcium system. Following the combination of the source of aluminosilicate and the alkali activator, the covalent Si-O-Si and Al-O-Si bonds present in the aluminosilicate are dissolved. Dissolution is followed by a polycondensation reaction with the monomers interacting to form longer chains [16]. A more detailed outline of the sequence of reaction processes as proposed by [17] can be seen in **Figure 3**. The main reaction product generated in the alkaline activation of these types of silica- and alumina- rich materials is an amorphous alkaline aluminosilicate hydrate known as N-A-S-H gel [15]. This N-A-S-H gel can be regarded as a highly crosslinked (mainly Q^4) zeolite precursor because it has a chemical composition similar to natural zeolitic materials but with a different structure [18]. The structure of this type of gel is shown in **Figure 4**. Where zeolites have an extensive crystalline structure, N-A-S-H gel is amorphous [19]. The structural formation of the N-A-S-H gel is influenced by the Si:Al ratio and alkali content.

The role of the charge-balancing alkali metal cations (i.e. Na^+, K^+) in the aluminosilicate structure of AACs is to overcome the inherent valency difference between Si and Al. These metal cations balance out the negative charge created with each introduction of a tetrahedral aluminum unit [19]. Currently the synthesis reaction for these materials requires a high pH, achievable with NaOH and KOH, which is why Na^+ and K^+ are the cations typically present in these systems [16].

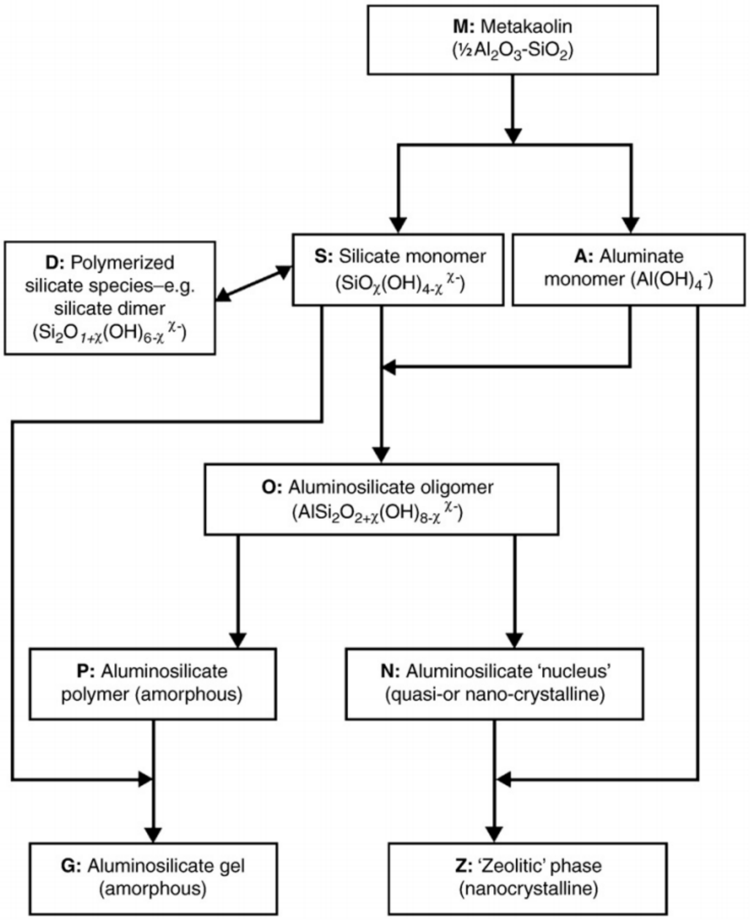

Figure 3. Proposed schematic outlining the sequence of reaction processes involved in the alkali-activation of metakaolin. [20]

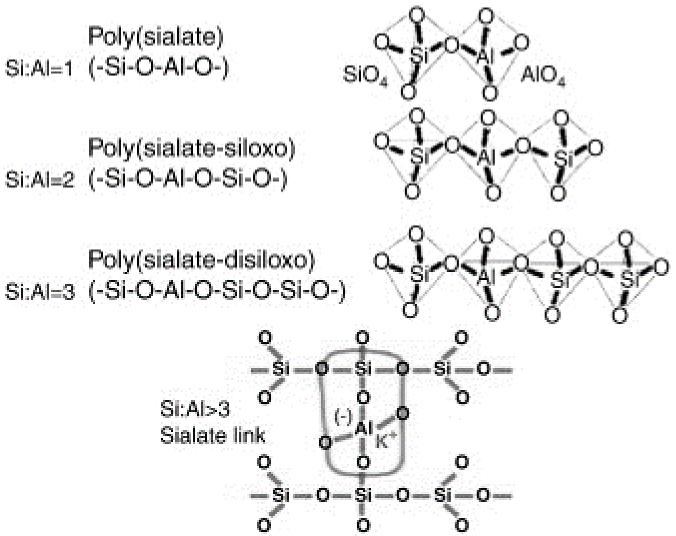

Figure 4. Structure of N-A-S-H gel [21]

2.3 DETERIORATION MECHANISMS RESULTING FROM ACID EXPOSURE

OPC, high-calcium AACs, and low-calcium or calcium free AACs differ in their responses to acid exposure because of their differing reaction products and microstructures. Below are descriptions of the deterioration mechanisms from acid exposure for each of these types of materials as they are currently understood.

2.3.1 OPC

When OPC pastes are exposed to acid, an ion exchange reaction occurs between the calcium cations present in the C-S-H binder gel and the hydronium ions (H_3O^+) from the acid. Calcium hydroxide $Ca(OH)_2$ and calcium sulphoaluminates present in the cement matrix are dissolved. This dissolution of $Ca(OH)_2$ and calcium sulphoaluminates and the decalcification of the C-S-H binder results in a corroded layer with a high porosity [17]. In the case of exposure to sulfuric acid, this porous corroded layer is composed primarily of gypsum due to the reaction of sulfate anions contributed by the acid and the liberated calcium cations.

2.3.2 High-calcium AACs

In AACs that contain some amount of calcium, corrosion due to acid exposure essentially occurs in two steps. In the first step, an ion exchange reaction occurs between cations of the framework (i.e., sodium and calcium) and hydronium ions from the acid solution. Acid protons also attack the Si-O-Al bonds which results in the ejection of tetrahedral aluminum from the aluminosilicate network (i.e., dealumination) [22]. In the second step, the exchanged calcium ions react with sulfate anions to form gypsum [22] in a similar manner to OPC.

2.3.3 Low-calcium AACs

In low-calcium AACs, the acid degradation mechanism occurs in a similar manner to that of high-calcium AACs, but the ion exchange reaction primarily occurs between the charge-balancing sodium cations (rather than calcium cations) and hydronium ions from the acid solution as shown in **Figure 5**. Following this exchange and the loss of the charge balancing cation, hydrolysis of Si-O-Al bonds results in the dissolution of tetrahedral Al [23][24][22]. This dissolution is known as dealumination and results in destabilization of the aluminosilicate framework. This dissolution also results in the formation of water as a by-product, increasing the solution pH [23]. Crystallization of zeolites can also occur [23].

Some studies have shown that silica dissolved from the binder or from zeolites that are present in the material can precipitate as silica gel at the acid corrosion front due to its low solubility at a low pH [24]. This precipitated silica gel could aid in the overall acid resistance of the material by clogging pores and inhibiting further dissolution [24].

While the basic mechanism behind deterioration due to acid exposure in low-calcium and calcium free AACs is understood, further research is needed to be able to better predict dissolution reactions of the AAC binders taking into consideration different Si:Al ratios and varying H_2O and cation contents [23]. Furthermore, very little testing has been done using metakaolin-based (or other calcium free) AACs.

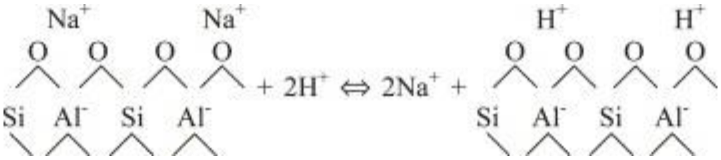

Figure 5. Replacement of exchangeable cations in polymers by hydrogen or hydronium ions following interaction with acidic solutions [22].

2.4 FACTORS AFFECTING AAC ACID RESISTANCE

As discussed in **Section 2.2**, the reaction mechanisms and products can vary greatly according to different factors in the mix design implemented, including as the type of precursor, the type and concentration of the chemical activator, and how long the material is allowed to cure and under what conditions. Because the durability of AACs largely depends upon the nature of reaction products, this section will serve to further elucidation of the factors influencing the nano- and microstructure of AAC binder gels.

2.4.1 Precursors

Several factors are known to influence the durability of alkali-activated cements exposed to acid. Some of the primary factors affecting acid resistance in these materials are related to the primary aluminosilicate source used in the formulation of the material. These factors include: calcium content, initial stability of the aluminosilicate framework, the type of corrosion products that may form from these systems, and initial bulk physical properties, such as permeable porosity.

One major factor influencing the acid resistance of alkali-activating cements is the nature and calcium content of the primary aluminosilicate source. Low-calcium-content cements created using an aluminosilicate source, such as class-F fly ash or metakaolin, have been shown to perform significantly better in acidic conditions compared to OPC [25]. In a similar study done by Bakharev comparing the acid resistance of OPC to alkali-activated slag concrete, the lower-calcium slag concrete performed better in the acidic environment, due to its lower free lime content.

The stability of the cross-linked aluminosilicate polymer structure is influenced by type of precursor and contributes to the acid resistance of AACs. In another study comparing the performance of blended ash geopolymer concrete and concrete made using OPC when exposed to sulfuric acid, results showed the geopolymer concrete to be more resistant to acid due to a more stable cross-linked aluminosilicate polymer structure [22]. The stability of the aluminosilicate structure, as well as the presence of active sites on the surface of the alumina silicate gel, also influence how the material will perform when in contact with aggressive media [21].

The rate of corrosion and the corrosion products formed upon acid exposure varies based on the type of precursor**.** In a study done by [26], OPC, alkali-activated blast furnace slag, and a lime-fly ash blend were tested in nitric acid and acetic acid. OPC pastes were found to have a higher corrosion rate than pastes made with slag or the lime-fly ash blend. In another study, [26] measured the corrosion rate of different inorganic polymer sample formulations subjected to sulfuric acid with a pH of 1.00. Samples made primarily with Class C (high-calcium) fly ash were significantly more resistant to acid than samples made using Class F (low-calcium) fly ash. In the same study, in samples made using GGBFS a corroded layer made up of gypsum formed. According to the study, this layer did not act as a barrier to diffusion [17]. However, in a different study, the deposition of gypsum crystals within the corroded layer appeared to offer a protective effect, acting as a barrier to the transport of ions across the corroded layer [26].

Permeable porosity is affected by the type of aluminosilicate source used and may contribute to the overall acid resistance of the material. In some cases, permeability and porosity appeared to be significant contributing factors in the performance of the cement [21], but in other cases porosity did not predict the performance of the material [13]. The effect of bulk physical properties on the durability of AACs in terms of acid resistance needs further study. More conclusive results could be established by designing experiments in such a way that statistical analysis could be done to determine the significance of these factors.

2.4.2 Chemical Activators

Another important factor involved in determining the properties of alkali-activated cements is the chemical activator used. Chemical activators can vary based on the alkali content, alkali type, state, and amount of dissolved silica content, all of which can be involved in determining the properties of the material, including the resistance to acid. One important difference in the effect these activating solutions can have is that NaOH activating solutions have a much higher pH than sodium silicate solutions of similar alkali concentrations. Strength development can differ with the chemical activator used as well. Silicate activated binders usually develop higher mechanical strength than NaOH-activated binders. This additional silicate species aids in the formation of denser N-A-S-H or C-A-S-H gel [14].

In a study by Lloyd et al., alkali content, alkali type, and dissolved silica content were varied. Increasing the alkali content (by increasing the amount of NaOH in the activating solution) had a strong influence on the reduction of the rate of corrosion of the material in sulfuric acid. In addition, the nature of the corroded layer changed as the alkali content increased. With an increase in alkali content, the development of shrinkage cracks became more prevalent in the corroded gel layer due to an increase in the amount of soluble material produced. The alkali type was varied between Na and K, but this appeared to have little significant effect on the rate of corrosion. In their study, the dissolved silica content was also varied through inclusion of sodium silicate in the activating solution. The additional silicate species introduced by the use of sodium silicate typically results in the formation of a denser N-A-S-H or C-A-S-H gel [22]. Samples activated with soluble silicate demonstrated superior acid resistance due to the denser microstructure created as a result of the presence of the soluble silica [13].

The structure and composition of the resulting gel product depends on the type of activator used. In another study in which the activating solution was varied between sodium silicate, NaOH, and KOH, it was found that the samples made using NaOH performed significantly better despite having a higher porosity [27]. The samples activated with NaOH had a more intrinsically ordered structure, contributing to the chemical stability of the polymers. In NaOH-activated slags, the C-A-S-H product has a higher Ca:Si ratio and a more ordered structure compared to the C-A-S-H gels formed as a result of NaSi activation of slag [19].

Alkali content has also been shown to affect the mineralization process and subsequent mineral formation which has the potential to affect the bulk physical properties of the material such as porosity [28]. In turn, the bulk properties of a material contribute to its acid resistance and overall durability.

2.4.3 Cationic Additions to AACs

The availability of network-modifying cations can have an effect on the durability of AACs. The effect of cationic exchange (and subsequent cation mobility) on the response of alkali-activated cements to different environmental conditions needs to be explored further. Studies have shown that an ion-exchange process can be used to replace the charge-balancing cations in aluminosilicate inorganic polymers with different cations in order to alter the properties of the material [28].

In a study done by [29], cation exchange materials were used to reduce the mobility of alkali cations in alkali-activated slag cements in order to stabilize the aluminosilicate framework. Vermiculite and 5A zeolite were introduced into the mix to remove mobile alkali cations. In order to determine the effectiveness of the cation exchange, the leaching of sodium was measured. The Na^+ leaching concentration was reduced significantly with the addition of the cation exchange materials. In that study, vermiculite proved to be a more effective cation exchange material in its ability to immobilize free Na+ ions and stabilize the aluminosilicate binder [30].

In addition to the use of cation exchange materials to alter the composition and properties of AACs, studies have shown that incorporating MgO within the binder has an effect on the development of the microstructure of alkali-activated materials. Walkley et al. completed studies in which MgO was incorporated into a synthetic precursor that was subsequently activated. The results of their investigation suggest that the availability of network modifying cations, such as magnesium, has an effect on the durability of alkali-activated cements by influencing microstructural changes occurring within the material when it is exposed to different aggressive environments [28].

2.5 SCOPE OF THE STUDY

The aim of this study is to systematically evaluate the effect of magnesium on the acid degradation response of calcium free AACs using a central composite design of experiments, in which the chemical composition of the binders are varied based on (1) silica content, (2) alkali content, and (3) magnesium-mineral content. This study hypothesizes that the introduction of a magnesium mineral in the form of brucite will increase the acid resistance of the material. The use of a central composite design enables statistical analysis and formation of models to describe the effect of magnesium on porosity change and elemental leaching of the material during acid exposure. In this study, AAC binders were exposed to sulfuric acid with a pH = 2.0 ± 0.05 to test different degradation theories. The method of sample preparation will utilize the natural precursor metakaolin in combination with sodium hydroxide and sodium silicate-based activating solutions. This study is designed to aid in the formulation of AACs that are more resistant to MICC by evaluating the effect of a specific mineral addition.

CHAPTER 3 MATERIALS AND METHODS

3.1 MATERIALS

Metakaolin (MK) (MetaMax) was supplied by BASF Chemical Corporation (Georgia USA). MK was chosen as the primary source of aluminosilicate-rich material in this study because it is a more chemically pure material than other commonly used aluminosilicate sources in AACs (such as fly ash), allowing for a greater understanding of the reactions occurring in the aluminosilicate binder gel. In addition, MK enables study of a calcium-free system. The chemical composition of MK as determined by ICP-OES is shown in Table 1:

Table 1: Chemical composition of MK in wt. %.

(wt.%)	**SiO_2**	**Al_2O_3**	**CaO**	**SO_4**	**Fe_2O_3**	**K_2O**	**Na_2O**	**P_2O_5**
Metakaolin	54%	47%	0.1%	0.3%	0.4%	0.1%	0.3%	0.1%

The alkali-activating solution used was prepared using sodium hydroxide (NaOH) (Sigma Aldrich, reagent grade) and sodium silicate (NaSi) (Sigma Aldrich, reagent grade). The magnesium addition to the AACs was provided in the form of brucite powder ($Mg(OH)_2$) (Sigma Aldrich, reagent grade).

After the AAC pastes were created, the samples were exposed to a sulfuric acid solution with a pH of 2.0 (±0.07). The sulfuric acid solutions were prepared by adding concentrated sulfuric acid (Sigma Aldrich, reagent grade) to deionized water.

3.2 CENTRAL COMPOSITE EXPERIMENTAL DESIGN

A central composite experiment was designed to explore the effect not only of magnesium mineral addition, but also the effects of alkali and silica contents, as well as interactions between them. Based on ranges explored in previous studies, the alkali (which, in this case, is sodium) to aluminum (Na:Al) ratio is varied between 0.5 and 1.5. Similarly, the silicon to aluminum (Si:Al) ratio is varied between 1 and 2. This range was chosen based on previous studies in which the binders shown to have the greatest mechanical strength were obtained with materials having a starting Si:Al ratio ranging from 1 to 2 [31]. For the magnesium-containing samples, brucite ($Mg(OH)_2$) was added to obtain a Mg:Si design ratio of 0.85, which was chosen to be within a range of values previously explored in the synthesis of magnesium silicate hydrate gels [32][28].

The design employed four cube points, four axial points, and one centerpoint (see **Figure 6**), such that a response surface model could be developed. The specific proportions and constituent materials for each mixture design formulation are shown in **Table 2**. This table also includes the Si:Al and Na:Al ratios evaluated which make up the central composite design in **Figure 6.** Diagram of central composite mixture designs showing the ranges of Si:Al and Na:Al ratios.

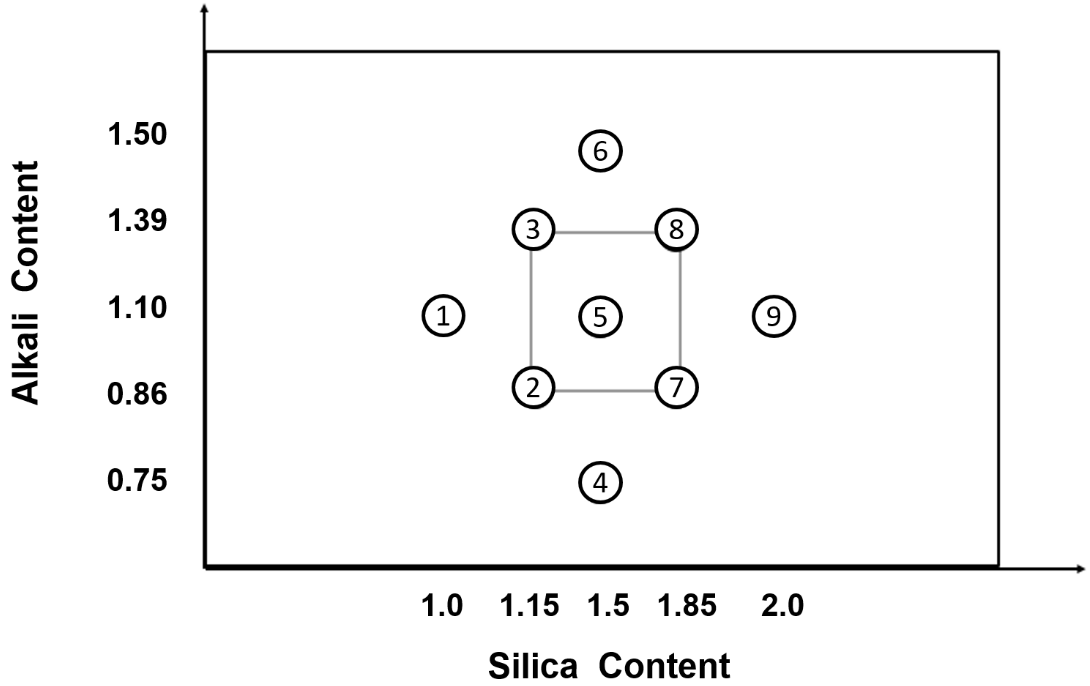

Figure 6. Diagram of central composite mixture designs showing the ranges of Si:Al and Na:Al ratios.

Table 2. Mixture proportions for metakaolin-based alkali-activated cement control and brucite addition samples.

Sample ID	**Constituent Materials**					**Important Parameters**		
Sample Name	MK (g)	$Mg(OH)_2$(g)	NaSi(ml)	NaOH (g)	$H_2$0 (ml)	Mg:Si	Si:Al	Na:Al
C1	50	0	0	20.1	56.5	0	1	1.1
C2	50	0	13.5	13	45	0	1.15	0.86
C3	50	0	13.5	22.8	45	0	1.15	1.39
C4	50	0	39	5.8	23	0	1.5	0.75
C5	50	0	39	12.8	23	0	1.5	1.1
C6	50	0	39	19.7	23	0	1.5	1.5
C7	50	0	64.5	2.7	1	0	1.85	0.86
C8	50	0	64.5	12.5	1	0	1.85	1.39
C9	50	0	75.5	4.9	0	0	2	1.1
B1	50	22.3	0	20.1	56.5	0.85	1	1.1
B2	50	26.4	13.5	13	45	0.85	1.15	0.86
B3	50	26.4	13.5	22.8	45	0.85	1.15	1.39
B4	50	34.3	39	5.8	23	0.85	1.5	0.75
B5	50	34.3	39	12.8	23	0.85	1.5	1.1
B6	50	34.3	39	19.7	23	0.85	1.5	1.5
B7	50	42.2	64.5	2.7	18	0.85	1.85	0.86
B8	50	42.2	64.5	12.5	18	0.85	1.85	1.39
B9	50	45.6	75.5	4.9	13	0.85	2	1.1

3.3 EXPERIMENTAL METHODS

3.3.1 Alkali-Activated Cement Sample Preparation

In this study, AAC paste samples were prepared using alkali-activating solutions composed of NaSi solutions with varying NaOH molar concentrations according to the prescribed mix design parameters shown in **Table *2***. Paste samples were used rather than mortars or concrete to eliminate any potential influence of aggregate.

Alkali-activating solutions were prepared for each sample to obtain the specified chemical ratios. NaOH pellets were first dissolved in the NaSi solution, adding necessary deionized water to achieve a consistent workability. Components were mixed in a closed container and the solutions were left to equilibrate in a refrigerator set to 4° C before mixing.

The alkali-activating solution described above and the metakaolin were mixed at room temperature using a Waring stand mixer. Mixing procedure consisted of an initial 1 min of manual mixing, followed by 1 min of mechanical mixing and 1 min of manual mixing to ensure that all of the dry components were incorporated into the mixture and evenly mixed. Then, samples were cast in molds (diameter 2.5 – 2.7 cm).

Paste samples were cured in sealed containers (99% RH) in a Quincy forced air laboratory oven for 48 hours at 40 °C. After initial curing, samples were demolded and cured 30 °C for an additional 24 hours.

3.3.2 Acid Exposure and Semi-Dynamic Leaching

Samples were exposed two times to a sulfuric acid solution with a pH of 2.0 (±0.07) until equilibrium was reached. The amount of acid solution used for each sample was determined based on a volume-to-surface-area ratio of 7 modified from ASTM C1308. Equilibrium was defined as solutions attaining pH changes less than 0.0025 per hour. After equilibrium was reached, the acid solutions were replaced and samples of the leachate media were analyzed via ICP-OES and ICP-MS.

3.3.3 Bulk Permeable Porosity

Permeable porosities were measured according to a vacuum saturation method modified from ASTM C1202. Volumes of the samples were calculated based on measurements of the height and diameter of the samples taken with calipers with an accuracy of 0.01 mm. Permeable porosity was calculated as the difference in SSD mass and OD mass normalized by the density of ethanol (0.803 g/cm^3) all divided by the total sample volume. All weights were recorded using a Mettler Toledo PL 1502E scale.

In order to obtain the oven dry (OD) weights of the samples, the samples were dried in a 70% wt. ethanol and 30% wt. tap water solution for 8 hours followed by submersion in 100 % wt. ethanol for an additional 8 hours and then dried in a Quincy forced air laboratory oven for 3 hours at 40 °C. To obtain the saturated surface dry (SSD) weight, samples were subjected to a vacuum while immersed in ethanol to allow the ethanol to fully infiltrate the sample. Ethanol was used as the liquid medium rather than water to ensure that there would be no further reaction between the AAC sample and water.

Due to the use of ethanol vacuum intrusion in this method, which may be destructive to the sample, measured porosity values may be higher than the actual values. However, because porosity was measured consistently across all samples, the porosity values relative to each other can still provide useful information.

3.3.4 X-ray Diffraction (XRD)

To determine mineralogy, flat disk samples were first crushed into a powder with a mortar and pestle. For semi-quantitative XRD, 800±0.5mg of the resulting powdered sample was mixed with 200 ± 0.5 mg of corundum (American Elements) as an internal standard and added to a mill capsule with clean, well-packed yttrium beads and 4-5 ml of ethanol. The mixture was then ground in a McCrone micronizing mill for 5 minutes. After the sample was ground, the resulting slurry was removed from the capsule and allowed to dry overnight in a laboratory oven at 60˚C. This milling process generates particle sizes with 95% below 30 mu.

The dried sample was then placed in a plastic scintillation vessel along with three Nylon beads and 0.4-0.5 ml of Vertrel. The scintillation vial was then placed in a SK-L330 Pro mechanical shaker and allowed to shake for 10 minutes. This step is used to encourage random particle orientation.

The sample was then filtered through a 250 mu screen and packed into XRD analysis plates. A Siemens D500 X-ray diffractometer was used to acquire diffraction patterns for all samples. The added corundum was used to normalize peak heights between samples and align diffraction patterns. Jade software (MDI, Version 9) was used to identify mineralogy.

3.3.5 Electron Microprobe Analysis (EMPA)

To examine the chemical composition of the paste samples and to visualize the corrosion front and diffusion of magnesium throughout the sample following acid exposure, electron microprobe analysis was used. Electron microprobe analysis is a non-destructive, *in situ* method of X-ray microanalysis and imaging of solid materials. To prepare the samples, they were first mounted in epoxy and placed under a vacuum to allow the epoxy to infiltrate the pores. The epoxy was then allowed to cure for 6 hours at ambient conditions and then 2 hours at 60° C. The samples were then ground using silicon carbide abrasive material with increasing grit numbers (i.e., 400, 600, 1200, 2000) followed by polishing with diamond suspensions until a 0.05 μm final polish was achieved. An Edwards Auto306 dual-coater was used to coat all samples with silver. For the analysis, a JEOL JXA-8230 electron microprobe with 5 wavelength-dispersive spectrometers was used.

The acceleration voltage and beam current used for all maps was 15keV and 100nA, respectively. The pixel size chosen for the maps was 6 um, which the electron beam was adjusted to match. A dwell time of 20 msec was used. The element maps produced were processed using the software CalcImage (ProbeSoftware, Inc.) in order to apply the mean atomic number background correction.

CHAPTER 4 RESULTS

4.1 VISUAL APPEARANCE

The visual appearance of the paste samples following exposure to sulfuric acid as shown in **Figure 7** indicates superior acid resistance in the samples with brucite addition. Most of the control samples exhibit some degree of exposure-induced cracking, while the samples with the magnesium mineral addition show little change before and after acid exposure. The exception to this trend is the mixture design formulation with a Na:Al ratio of 0.86 and Si:Al ratio of 1.85. In this case, the sample with a brucite addition cracked under acid exposure while the control sample remained intact. This cracking is attributable to exacerbated shrinkage cracking, as elucidated in **Section 4.2**.

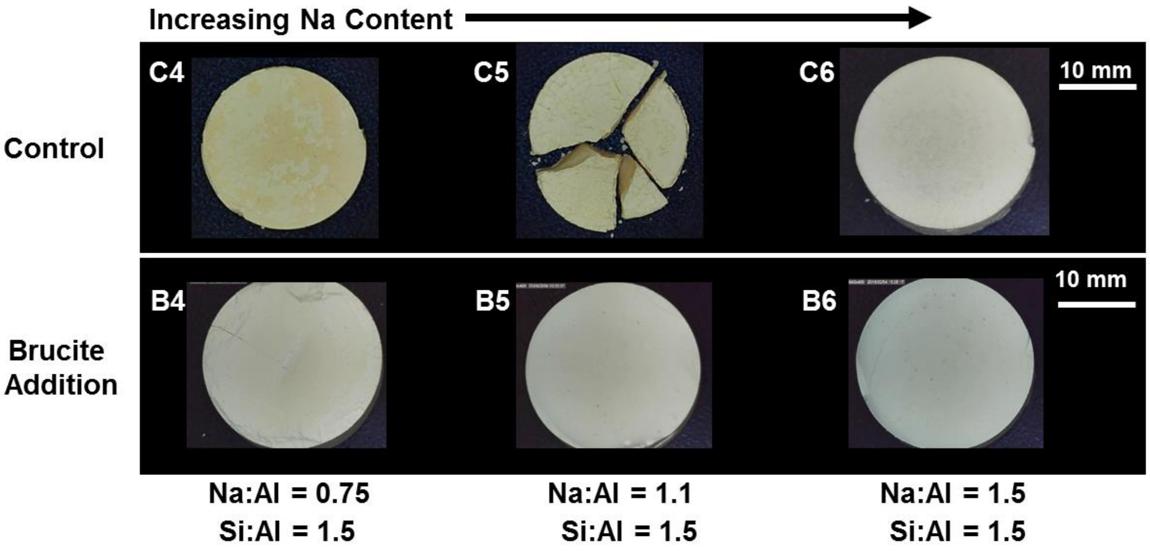

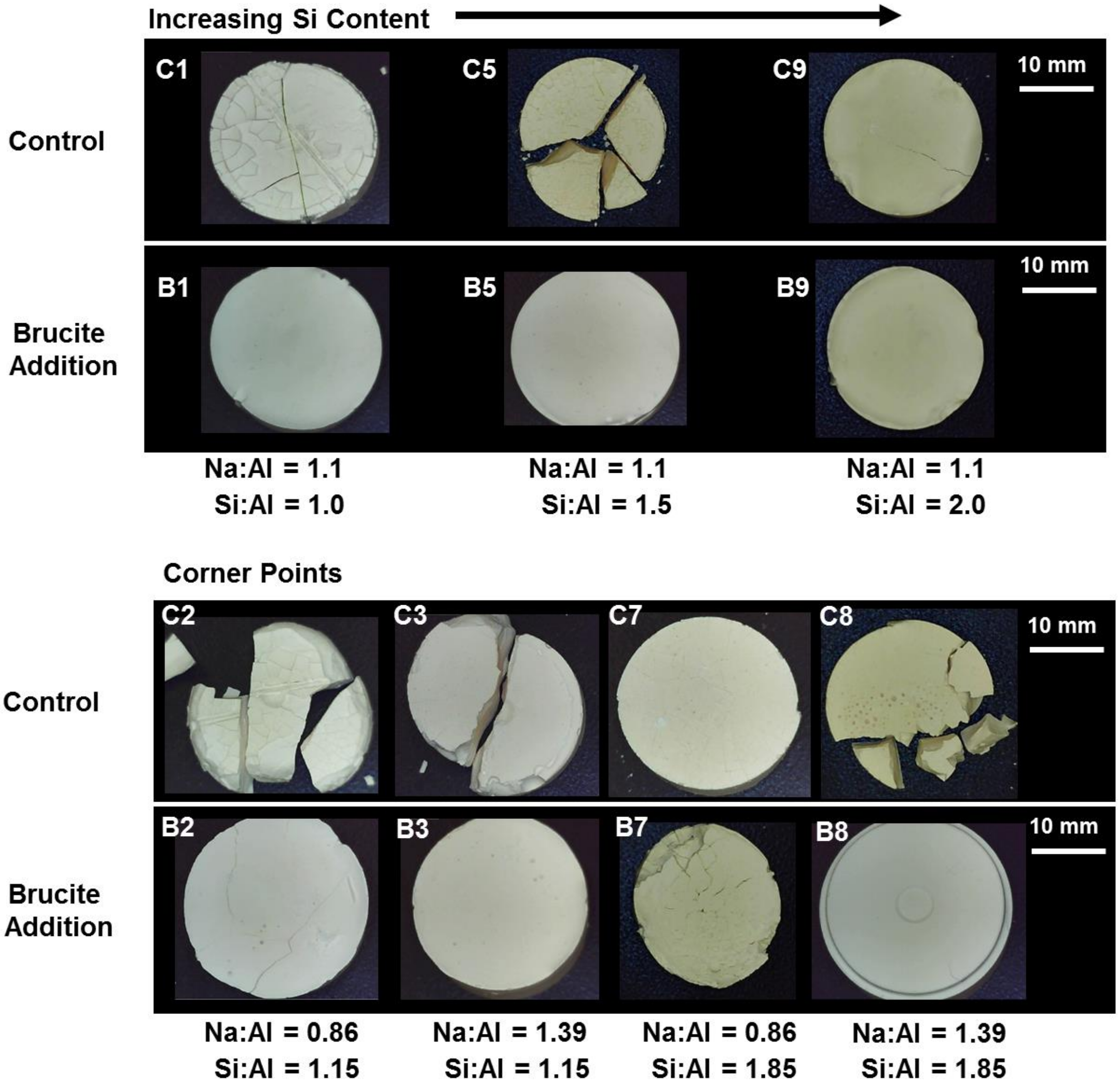

Figure 7. Control and brucite addition samples after acid exposure arranged in terms of increasing sodium content, increasing silica content, and the cornerpoints of the central composite design.

4.2 SHRINKAGE

In addition to evaluating the visual appearance of the samples, shrinkage was measured by comparing the diameter of the sample before and after curing. The percent change in diameter for each sample formulation is shown in terms of increasing silica content in Figure 8 below. In most cases, the samples with brucite addition experience similar or less shrinkage than the control samples. The exception to this trend is the Mg-containing sample (Na:Al = 0.86, Si:Al = 1.85) that experienced exacerbated shrinkage cracking.

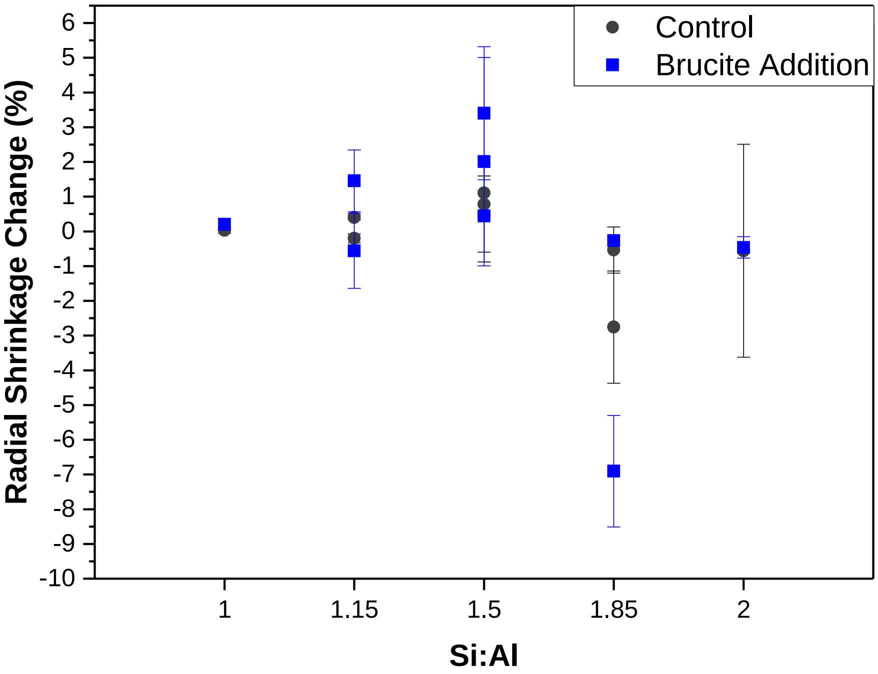

Figure 8. Percent change in diameter of control and brucite addition samples after curing. Negative values for percent change in diameter represent shrinkage in the sample.

4.3 MINERALOGY

The mineralogical profiles of the AAC samples before and after acid exposure are shown in **Figure 9** and **Figure 10. Table 3** summarizes the minerals observed and identified with XRD as well as their corresponding unit geometry, volume, and density according to each reference standard PDF noted from the Jade 5 mineral database. The symbols correspond to the peaks identified in **Figure 9** and **Figure 10**.

Upon acid exposure, there appears to be very little change in the mineralogy of the samples. In addition, the mineralogy of the control samples and the samples with Mg addition is the same for each mix design formulation, aside from brucite in the latter, as expected. All samples appear to be amorphous, except for mixture designs C1 and B1 and C3 and B3. In samples C1 and B1 (Na:Al = 1.10, Si:Al = 1.0), ordered Zeolite A and Sodium Aluminum Silicate Hydrates are formed. In sample C3 and B3 (Na:Al = 1.39, Si:Al = 1.15), Faujasite-Na is formed. The effect of this mineral formation on the bulk properties of the samples, as well as the performance of the sample during acid exposure, will be discussed in **CHAPTER 5**.

Table 3. Minerals identified in XRD results and the corresponding symbols used in their designation in the XRD patterns.

Mineral name	**Stoichiometry**	**Symbol**	**Unit Geometry**	**Unit cell volume (Å^3)**	**Density (g/cm^3)**	**PDF #**
Brucite	$Mg(OH)_2$	B	Hexagonal	40.94	2.52	01-083-0114
Sodium Aluminum Silicate Hydrate	$Na_{96}Al_{96}Si_{96}O_{384}$ x $216H_20$	H	Cubic	14905.1	2.13	00-039-0222
Zeolite A	$Na_8Mg_2Al_{12}Si_{12}O_{48}(H_20)_{.75}$	A	Cubic	14570.41	2.67	01-084-0838
Corundum, syn.	Al_2O_3	C	Rhombohedral	254.81	3.39	00-046-1212
Faujasite-Na	$Na_{1.84}Al_2Si_4O_{11.92}$ x $7H_20$	F	Cubic	15034.47	1.94	00-039-1380
Sodium Carbonate	Na_2CO_3	S				00-018-1208

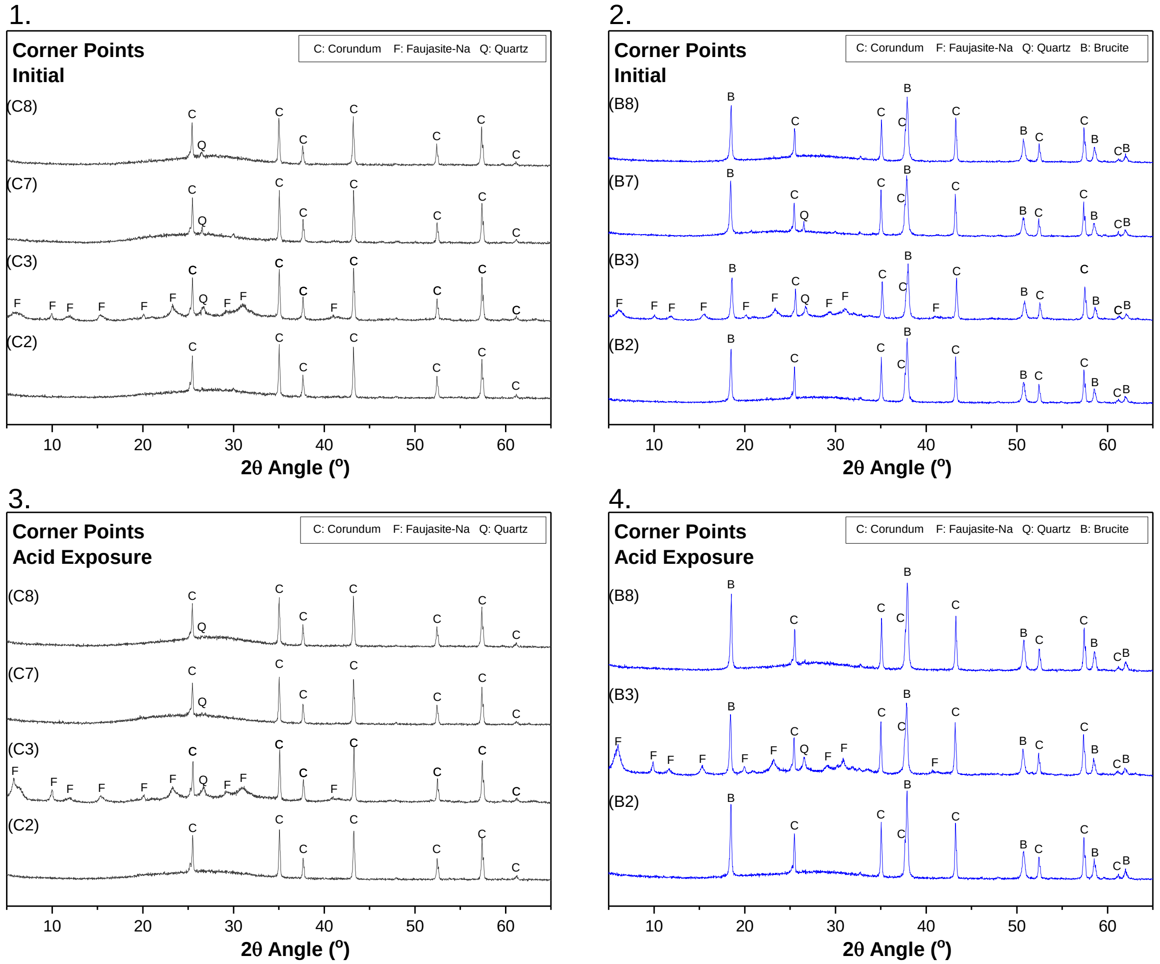

Figure 9. XRD patterns separated according to the central composite design formulations into corner points (1) control corner points, (2) brucite-containing corner points, (3) control corner points after acid exposure, and (4) brucite-containing corner points after acid exposure. Additional XRD patterns for amorphous samples can be found in the supplementary information.

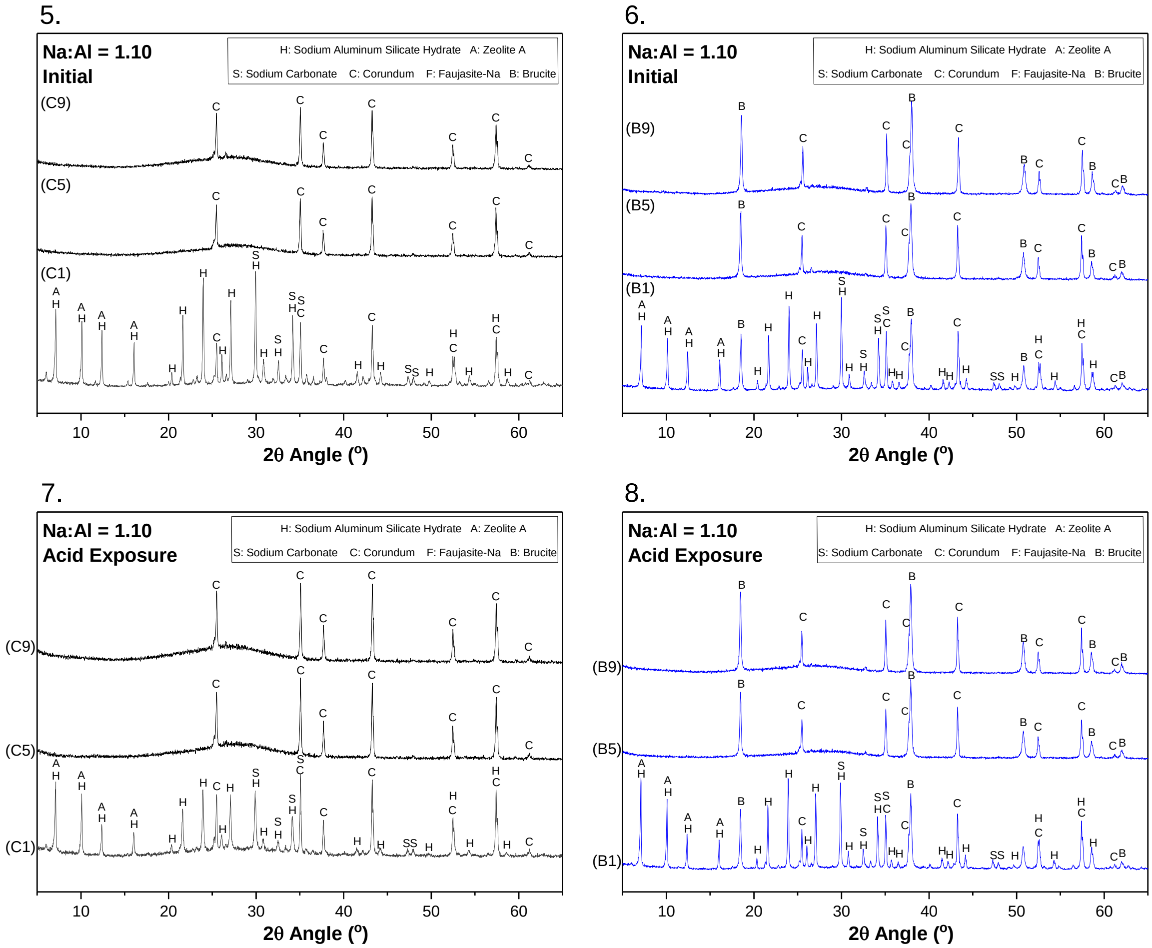

Figure 10. XRD patterns separated according to the central composite design formulations into increasing Si content points (5) control points, (6) brucite-containing points, (7) control points after acid exposure, and (8) brucite-containing points after acid exposure. Additional XRD patterns for amorphous samples can be found in the supplementary information.

4.4 SEMI-DYNAMIC LEACHING

The leaching behaviors of all samples exposed to a sulfuric acid solution (pH = 2.00 ± 0.05) are shown in **Figure 11** The behavior for both equilibrium sets is shown, as well as the behavior of the samples with and without brucite addition. The effect of Na content and Si content are evaluated in the following sections that discuss the leaching of each element. These effects help explain the wide range in leaching concentrations observed in the results. In order to account for the reduction in silica and aluminum in the brucite addition samples (due to the volume in each sample taken up by the added brucite), the leaching data were normalized by weight percent of the binder. For example, the weight percent binder is 100% in the control samples and 85% in the brucite addition samples.

Formulations containing brucite exhibited a reduction in leaching of Si, Al, and Na from the first equilibrium set to the second. This observation is based on the boxplots shown in **Figure 11**. On the other hand, the leaching of Mg increased by a factor of 7.2 on average during the second equilibrium. On the other hand, the leaching of Al in the control samples showed little variation between equilibrium sets and, while Si leaching decreased in the second set, the reduction is less apparent than in the samples containing brucite. Na leaching in control samples decreased by approximately 72% between equilibrium sets in comparison to a decrease of 60% in the brucite-containing samples.

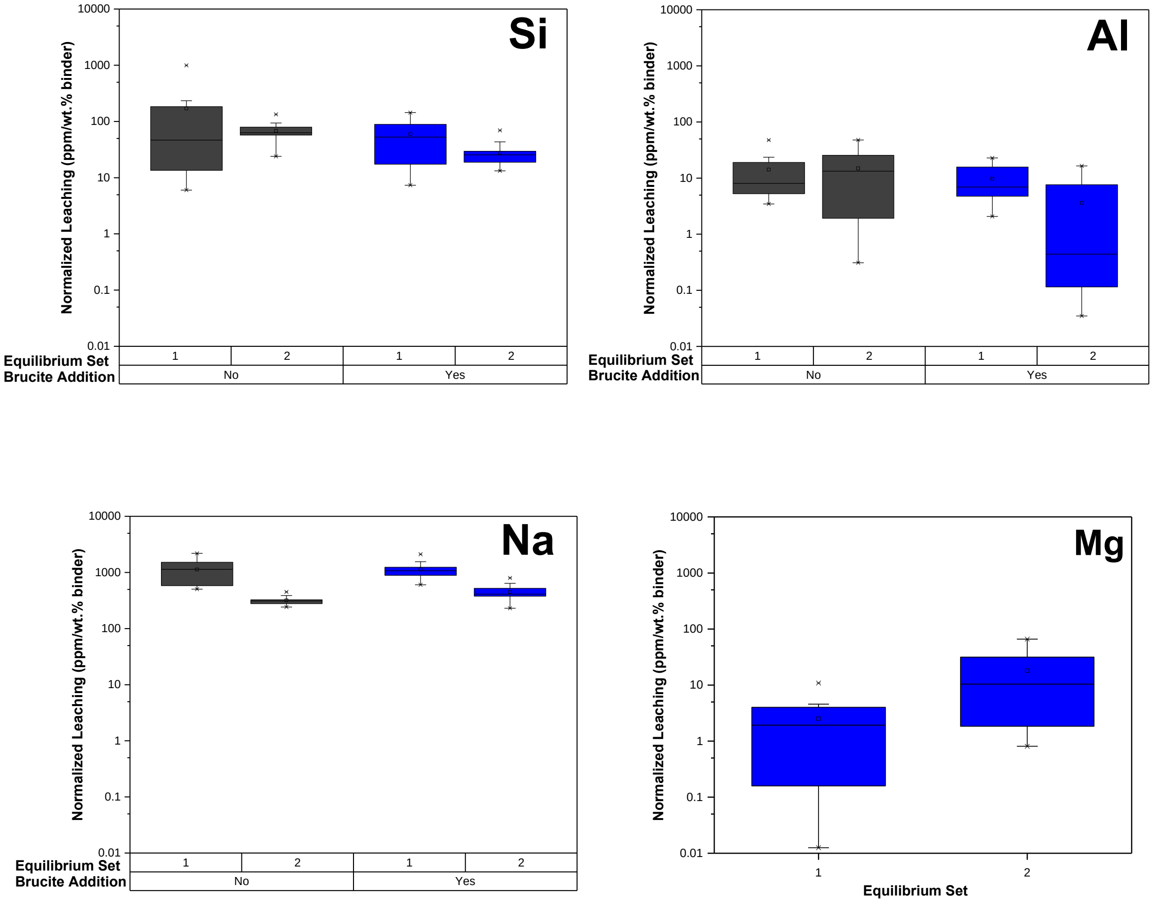

Figure 11. Leaching data in sulfuric acid (pH = 2.00 ± 0.05) normalized by wt. % binder (to account for the brucite addition) for two equilibrium sets for all mix design formulations for both control and brucite addition samples (except in the case of magnesium leaching).

In addition to the boxplots shown above, response surfaces were developed based on the results of the central composite design for elemental leaching (of sodium, silicon, aluminum, and magnesium). The adjusted squared regression coefficient is reported for each set of response surfaces. In the case of each of the leaching models, the data were transformed via a Box-Cox transformation ($\lambda = 0$) to approximate a natural log behavior of the data. The data transformation was validated based on the residuals and fits plots as well as an improved squared regression coefficient. Residuals and fits plots are shown in the **Supplementary Information**.

The response surfaces for the leaching of sodium shown in **Figure 12** indicate that the least amount of Na leaching occurs in samples with Na:Si ratios of ≈ 0.75. The highest amount of Na leaching occurs in samples with low silica contents in combination with high sodium content as well as in samples with high silica contents and low sodium content.

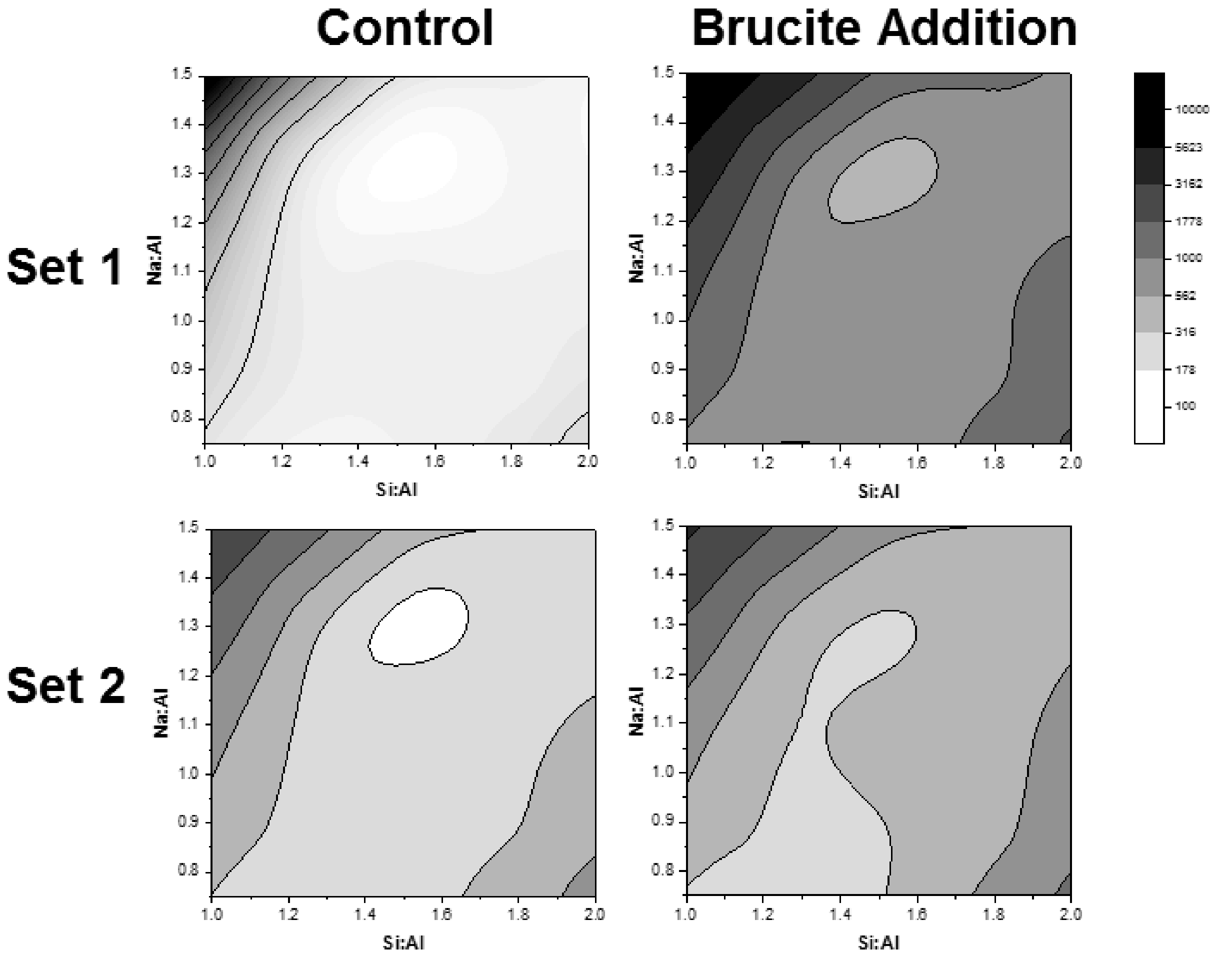

Figure 12. Response surface for the leaching of sodium for each equilibrium set and for both control and brucite addition samples. The scale bar to the right shows that a darker shade indicates a higher concentration (ppm) of sodium leached.

The silica leaching response surfaces in **Figure 13** suggest that the lowest leaching of silica occurs in formulations with low silica content and low sodium content in the first equilibrium set. This result is also apparent in the second equilibrium set, which represents a more continuous acid attack. However, as with the leaching of Na, the least amount of Si leaching occurs in samples with formulations with Na:Si ratios of around 0.75. Based on the boxplots showing leaching data in **Figure 11** as well as the response surfaces (**Figure 13**), the addition of brucite does not have an apparent effect on the leaching of Si in the first equilibrium set. However, Mg does lead to a slight decrease in Si leaching in the second equilibrium set.

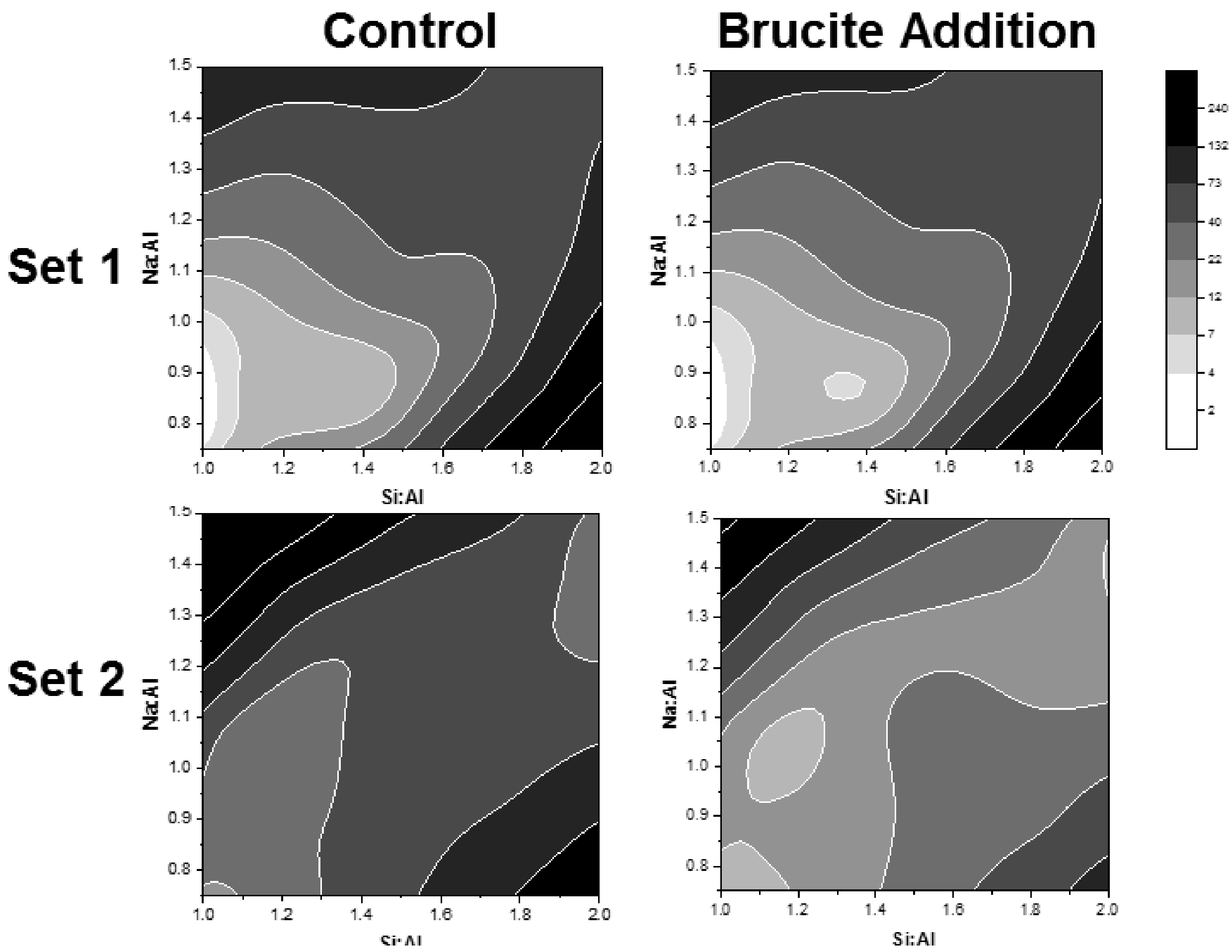

Figure 13. Response surface for the leaching of silicon for each equilibrium set and for both control and brucite addition samples. The scale bar to the right shows that a darker shade indicates a higher concentration (ppm) of silicon leached.

The response surface models for the leaching of aluminum in **Figure 14** show that in control samples, the greatest amount of leaching occurs in samples with low silica content, while in brucite-containing samples, the greatest amount of leaching occurs in samples with high silica content. For both control and brucite-containing samples, silica content plays a greater role in the first equilibrium set than in the second, in which the interaction between silica and sodium becomes more important. In addition, the brucite addition leads to a reduction in the leaching of aluminum in the second equilibrium set.

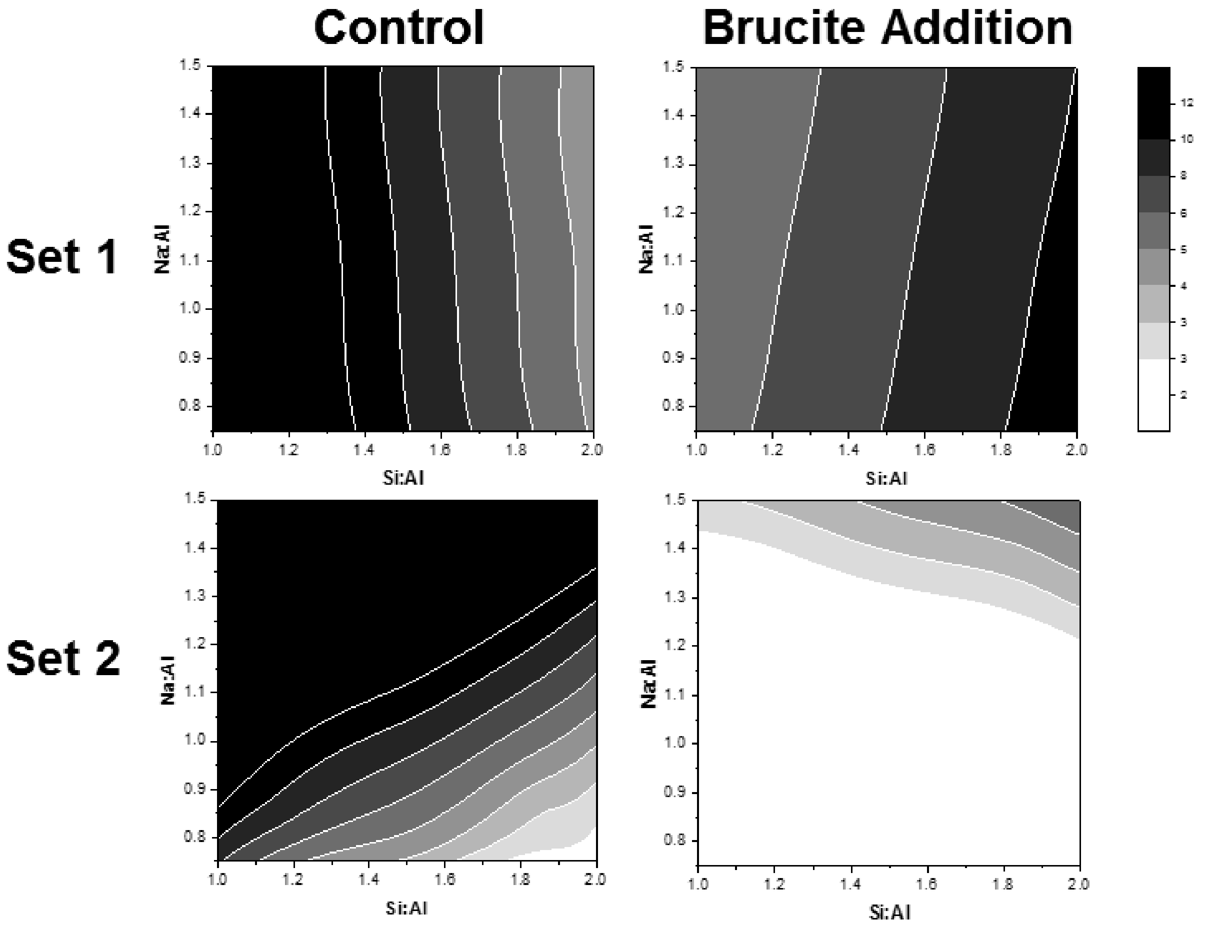

Figure 14. Response surface for the leaching of aluminum for each equilibrium set and for both control and brucite addition samples. The scale bar to the right shows that a darker shade indicates a higher concentration (ppm) of aluminum leached.

The response surfaces in **Figure 15** show that magnesium leaching increases between equilibrium sets, as expected. In addition, magnesium leaching decreases with an increase in sodium content.

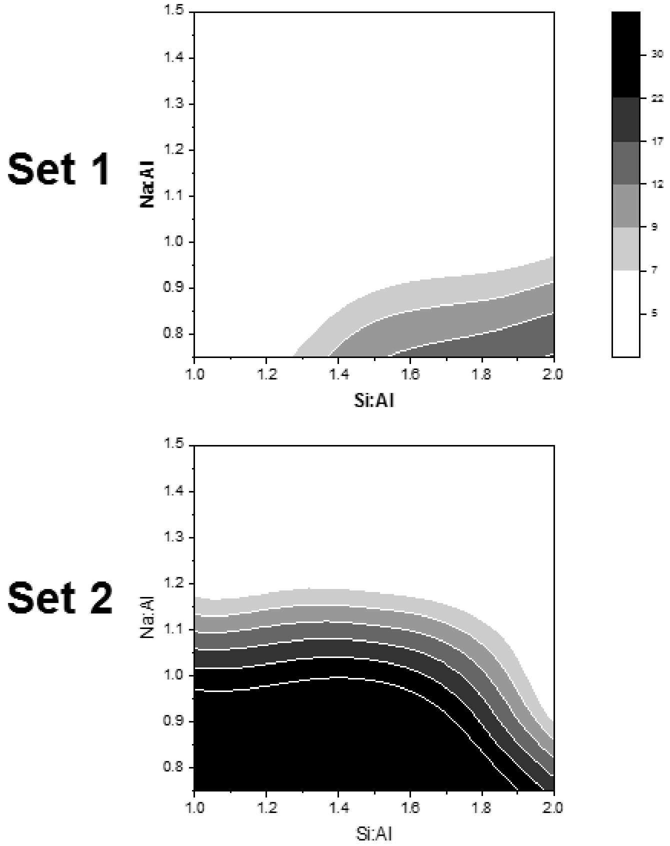

Figure 15. Response surface for the leaching of magnesium for each equilibrium set and for brucite addition samples. The scale bar to the right shows that a darker shade indicates a higher concentration (ppm) of magnesium leached.

In addition to measuring elemental leaching following each equilibrium set, the equilibrium pH for each mix design formulation was also recorded. The results comparing the equilibrium pH for control and brucite-containing samples for each set are shown in **Figure 16** below. Equilibrium pH is similar for all samples in the first exposure to acid, regardless of Mg content. In the second exposure to acid, the solutions from the brucite-containing samples maintain a higher pH.

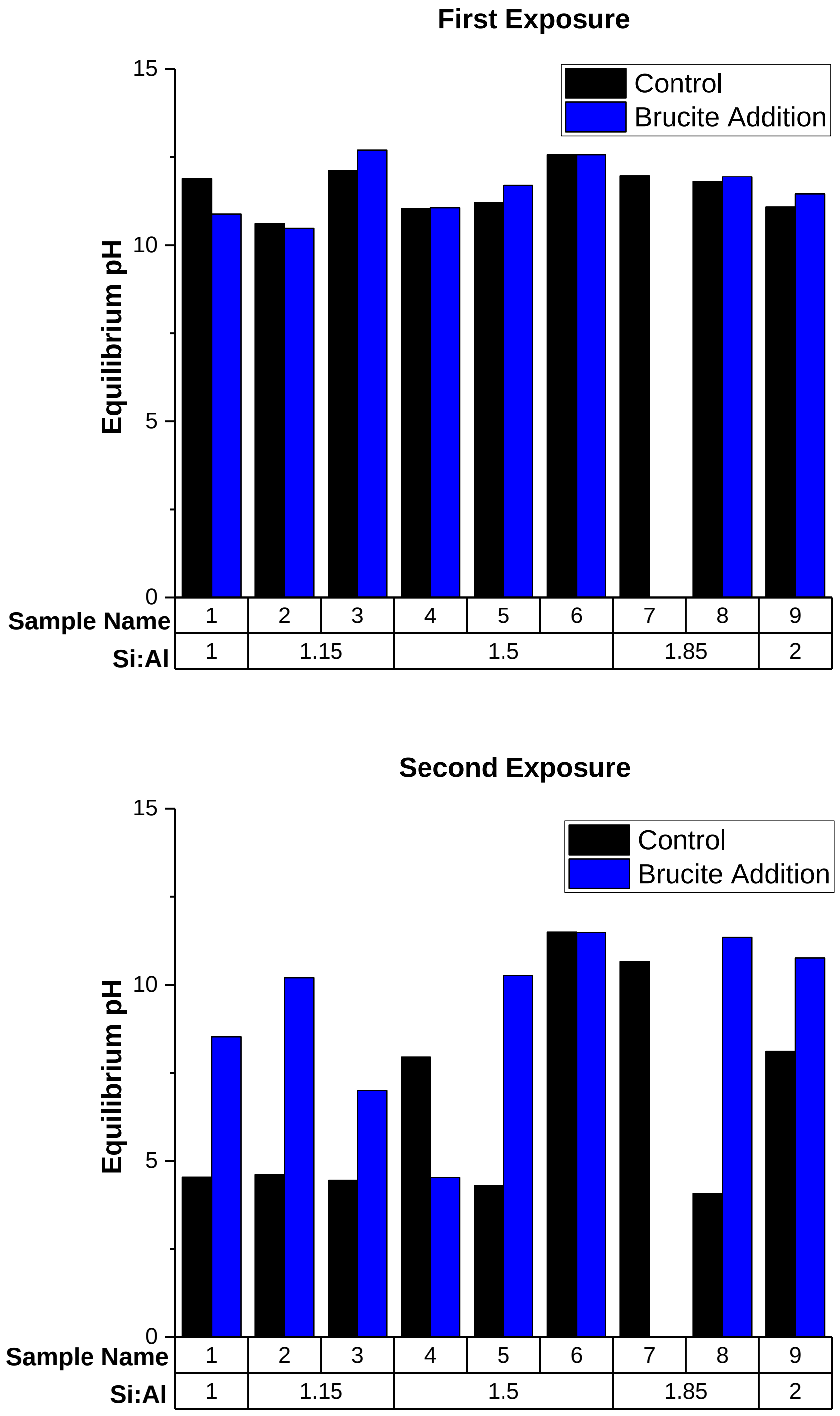

Figure 16. Equilibrium pH for each sample formulation for each exposure, displayed with increasing silica content from left to right.

4.5 PERMEABLE POROSITY

Brucite-containing samples exhibited lower initial porosities than control samples. After exposure to sulfuric acid, all samples experienced some increase in porosity. However, the porosity in the brucite-containing samples remained lower than the control samples. In addition, the samples including brucite experienced less change in porosity. To validate the observations made for each of these box plots, t-tests were performed to evaluate the difference between the control and brucite addition samples. The results of these tests show that the brucite addition does significantly reduce the initial porosity and porosity after acid exposure.

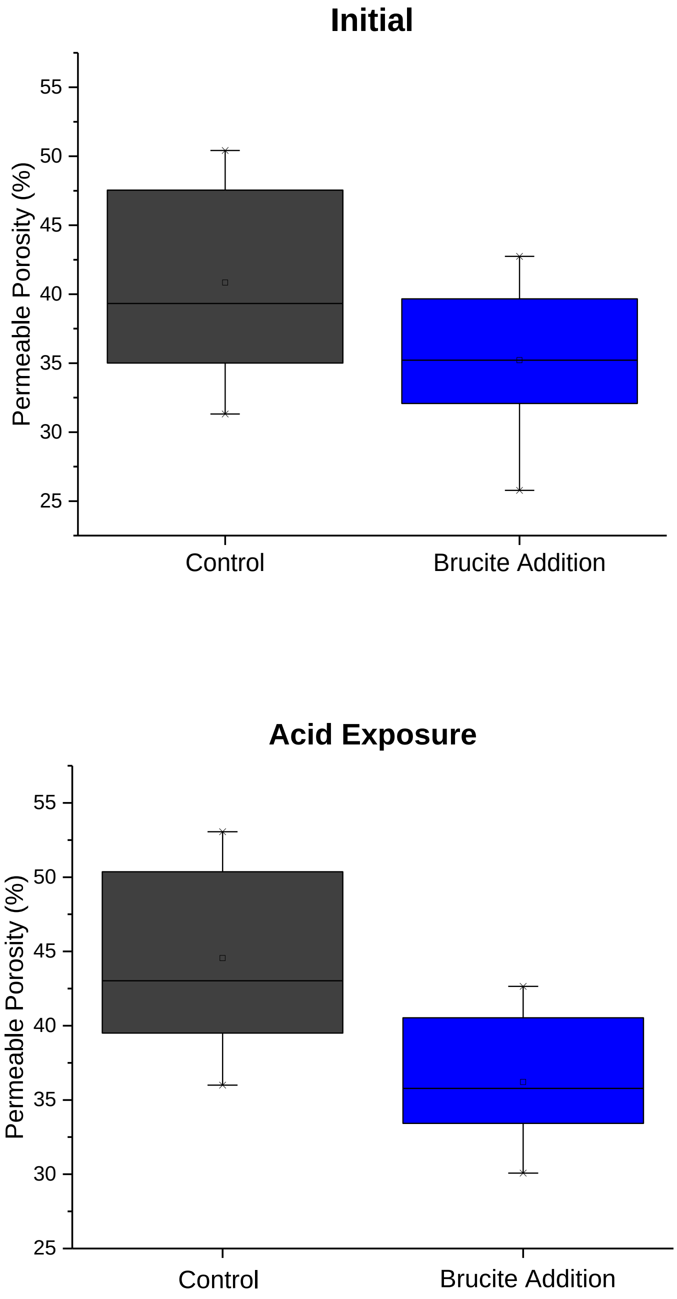

Figure 17. Porosity data in for control and brucite addition AAC samples before and after acid exposure for all sample formulations.

The response surface models shown in **Figure 18** were developed to evaluate the effect of silica and sodium content on porosity before and after acid exposure for both control and brucite-containing samples. Samples with brucite addition exhibit lower permeable porosity values than the control samples both before and after acid exposure.

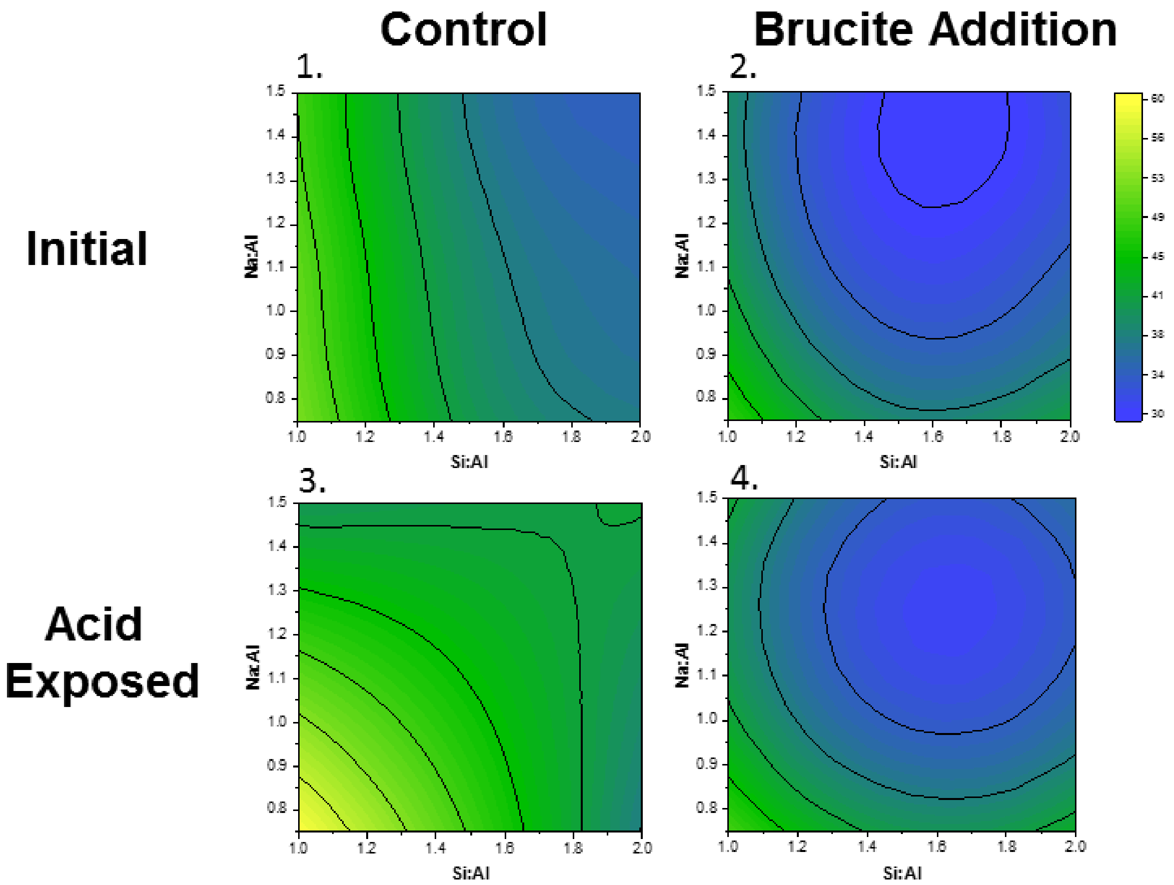

Figure 18. Response surface for permeable porosity of AAC samples with (1) initial porosity of control samples, (2) initial porosity of brucite addition samples, (3) porosity of control samples after acid exposure, and (4) porosity of brucite addition samples after acid exposure.

4.6 ELEMENTAL MAPS

Initially, elemental maps were created for each of the corner points for both control and brucite addition samples before and after acid exposure. However, 3 of the 4 control corner point samples failed during acid exposure (samples C2, C3, and C8, as can be seen in **Section 4.1**) and 1 of the 4 brucite-containing corner point samples failed during acid exposure (sample B7). Therefore, it was determined that the failed sample formulations were less acid-resistant than the others, and only the samples that were still intact were analyzed using EMPA. **Figure 19** shows the elemental maps for the control sample formulation, C7. The net-count color intensity scales for the maps are provided for each element.

In the elemental maps for the control sample exposed to acid, the corrosion front is apparent, and the sample behaves as expected. More explicitly, upon acid exposure, dealumination, a decrease in sodium atoms, and silica gelation can be observed at the corrosion front (see **Figure 19**).

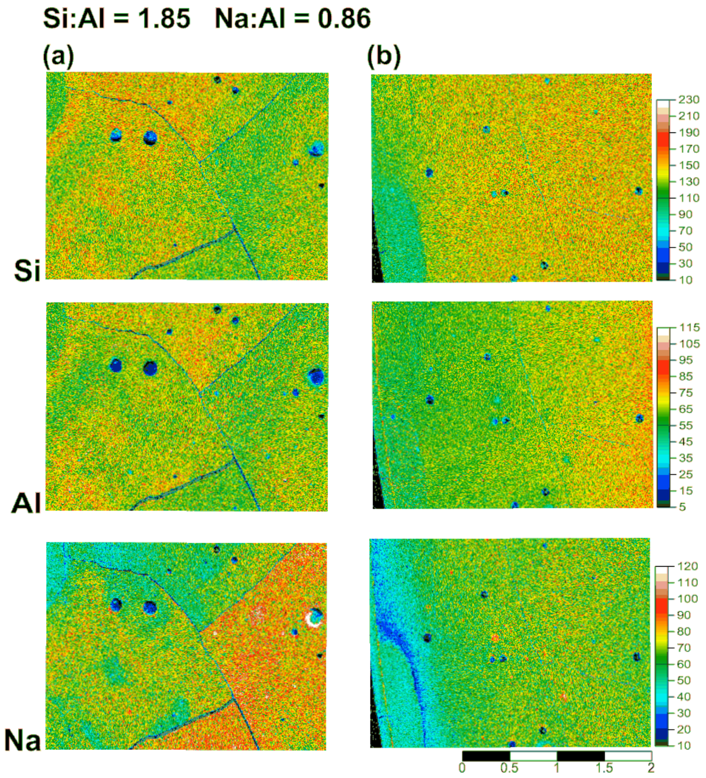

Figure 19. Elemental maps for control sample C7 (Si:Al = 1.85, Na:Al = 0.86). Samples before acid exposure are shown in column (a) and samples after exposure are shown in column (b). Acid intrusion is from the left. Scale bar = 2 mm.

In the samples containing brucite (**Figure 20**), the corrosion front is less apparent for elemental maps other than sodium. In sample B2, the corrosion front can be observed based on the reduction in sodium atoms at the edge of the sample and dealumination in some locations. In sample B8, while the corrosion front is not as clearly defined as in the control sample, it can still be observed. There does not appear to be evidence of dealumination in this sample, but there is a reduction in sodium atoms and apparent silica gelation at the corrosion front.

Furthermore, in **Figure 20** in the areas where there is a lack of sodium atoms after acid exposure, the concentration of magnesium appears to increase. There also appears to be a slight increase in the concentration of Mg throughout the sample after acid exposure. Because the quantity of brucite added in this study was so great, however, it is difficult to evaluate differences in the Mg elemental maps before and after acid exposure.

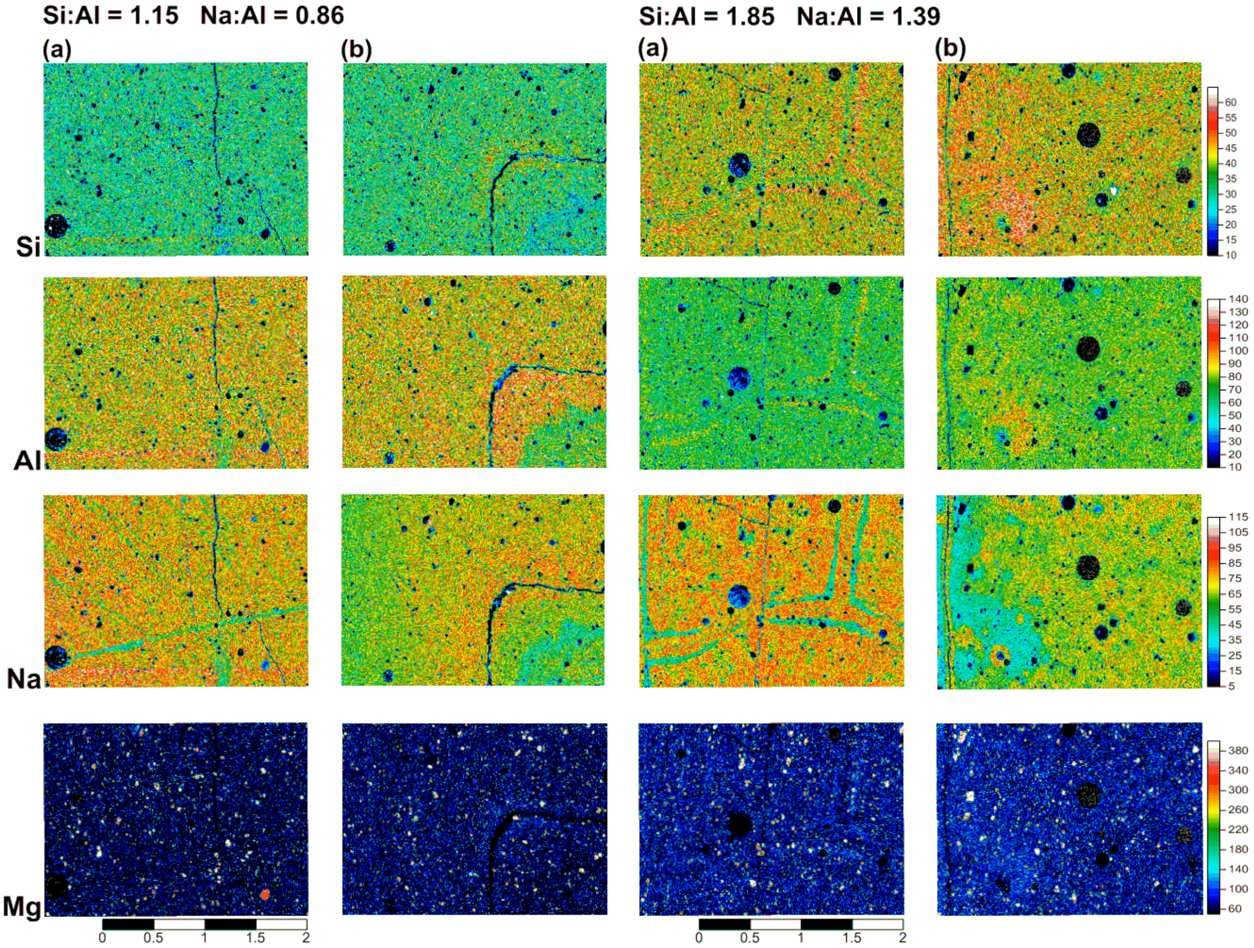

Figure 20. Elemental maps for sample formulations with brucite, B2 (Si:Al = 1.15, Na:Al = 0.86) and B3 (Si:Al = 1.85, Na:Al = 1.39). Samples before acid exposure are shown in column (a) and samples after exposure are shown in column (b). Acid intrusion is from the left. Scale bar = 2 mm.

CHAPTER 5 DISCUSSION

The addition of brucite contributes key differences to the response of MK-based AACs upon acid exposure. These affected factors included porosity, leaching quantities, and equilibrium pH. The overall impact of these factors resulted in an increase in the overall acid resistance compared to samples without brucite.

Brucite addition not only reduces initial porosity, but also reduces porosity after acid exposure. Samples with brucite did not experience as great an increase in porosity as the control samples after acid exposure. In a few formulations, the porosity of the samples actually decreased, implying a possible densification of the corrosion layer.

The brucite addition also reduces the importance of alkali content, as previously noted. Previous studies evaluating the acid resistance of AACs have shown that with the leaching of charge-balancing cations, the tetrahedral aluminum from the aluminosilicate framework is ejected and cracks begin to form [33]. With the brucite addition reducing the importance of the initial alkali content of the material, this indicates that the material is less reliant on sodium to act as a charge-balancing cation in the aluminosilicate framework when magnesium is present. Changes in porosity following acid exposure in the brucite-containing samples are not as dependent on either alkali content or the interaction between silica and sodium content as the control samples. In the models developed to describe porosity, silica and alkali content play different roles in the control versus brucite-containing samples. In the initial porosity response surface for the control samples, only silica content is important in determining porosity. An increase in silica corresponded to a decrease in porosity. However, in the response surfaces created for porosity after acid exposure, sodium content and the interaction between silica and sodium appeared to have a greater effect. One explanation for this is that the difference in excessive mobile alkali ions within the material between formulations becomes more important when the samples are exposed to an aggressive solution.

On the other hand, in samples containing brucite, the interaction between sodium and silica for both the initial and acid exposed porosity does not appear to have an effect on the porosity. Building off of the explanation previously mentioned, brucite may be affecting the aluminosilicate structure in such a way that the interaction between sodium and silica becomes less important. According to a previous study, when metakaolin is activated with sodium hydroxide or a combination sodium hydroxide and sodium silicate solution, some alkalis remain mobile rather than fixed into the aluminosilicate structure [23]. These alkalis are then easily dissolved, resulting in increases in porosity. However, if magnesium cations can replace these alkalis, then this would explain why the sodium content as well as its interaction with silica does not play as large a role in changes in porosity upon acid exposure.

In two cases, variations in silica and alkali content resulted in mineral formation, which affected the acid resistance of the material. The two main minerals that were formed included Zeolite A for formulation C1 and B1 samples and Faujasite-Na for formulation C3 and B3 samples. Following XRD analysis, the formation of these minerals was included as categorical variables in the analysis of the change in porosity and leaching data. Samples in which Faujasite-Na formed result in reduced porosity changes during acid exposure. Based on the XRD data, there is probable Faujasite-Na crystallization following acid exposure in both C3 and B3 samples. This could contribute to the reduced change in porosity in the mixture formulations in which Faujasite-Na developed, as previous studies have shown that early Faujasite-Na formation results in reduced porosity [27][34].

An additional effect of the variation in silica content can be seen in the shrinkage data. In samples in which NaSi was used as the primary activator, shrinkage increased, which also resulted in the failure of one of the magnesium-containing samples (B7), which had the lowest amount of NaOH:NaSi used in the activating solution.

Upon the second equilibrium exposure to acid, brucite addition emerges as an important factor in the reduction in the leaching of silica and aluminum, providing evidence that fewer Si-O-Al bonds in the binder are being broken. In order to determine whether or not the lower initial porosity of the brucite samples explained the reduced leaching of silica and aluminum, the effect of porosity on the leaching data collected needed to be evaluated. The permeable porosity data was plotted against the Si, Al, and Na leaching concentrations to see if an increase in porosity corresponded with higher leaching values, in which case porosity would be considered a covariate in the analysis of the leaching data. As can be seen in **Figure**

21, not all of the samples show a clear trend indicating an increase in leaching with an increase in porosity. However, for the samples in which the Si:Al ratio is 1.5, silicon and aluminum leaching does appear to increase with the increase in porosity of the samples. For this same set of mixture designs, the brucite-containing samples consistently have both lower porosities and lower silicon and aluminum leaching concentrations than the control samples. Therefore, for this study, while the results indicate that the reduced porosity of the brucite-containing samples is not the sole factor aiding in the reduction in silica and aluminum being leached, it is a contributing factor. In further studies, maintaining a more consistent porosity across sample sets by ensuring the same water to binder ratios would be beneficial in clarifying the role of porosity versus the role of the brucite addition in reducing leaching.

In order to determine the significance of the brucite addition on the leaching data shown in the box plots depicted in **Section 4.4**, t-tests were performed for each equilibrium set. This analysis showed that, for the first exposure, the difference in the amount of silica and aluminum leached between control and brucite addition samples was not significant. However, the brucite addition did significantly reduce the amount of silica and aluminum leached in the second exposure.

As can be seen in **Figure 21**, not all of the samples show a clear trend indicating an increase in leaching with an increase in porosity. However, for the samples in which the Si:Al ratio is 1.5, silicon and aluminum leaching does appear to increase with the increase in porosity of the samples. For this same set of mixture designs,

the brucite-containing samples consistently have both lower porosities and lower silicon and aluminum leaching concentrations than the control samples. Therefore, for this study, while the results indicate that the reduced porosity of the brucite-containing samples is not the sole factor aiding in the reduction in silica and aluminum being leached, it is a contributing factor. In further studies, maintaining a more consistent porosity across sample sets by ensuring the same water to binder ratios would be beneficial in clarifying the role of porosity versus the role of the brucite addition in reducing leaching.

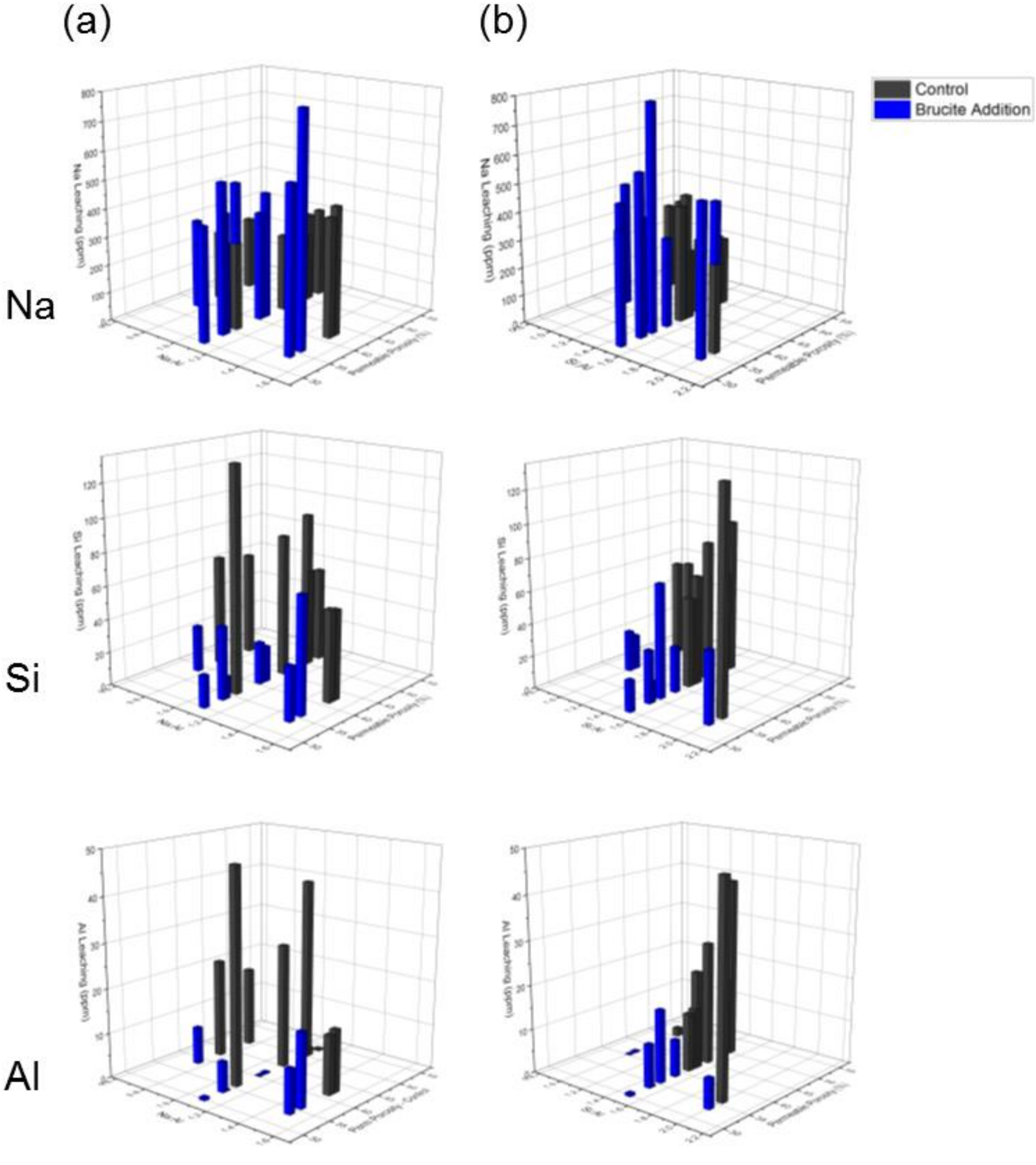

Figure 21. Sodium, silicon, and aluminum leaching data plotted against permeable porosity, (a) Na:Al ratio, and (b) Si:Al ratio for control and brucite-containing samples.

In the same plots shown in **Figure 21** for the brucite-containing samples, Na leaching appears to decrease despite an increase in porosity. Within the set of brucite-containing samples, this trend is largely due to the variance in the Na:Al ratios, which show that for higher amounts of sodium content, sodium leaching is increased. However, this does not fully explain why brucite-containing samples with consistently lower porosities would experience greater sodium leaching than the control samples. This trend may be attributable to the fact that the leaching data presented corresponds to the second equilibrium set (when porosity for the samples was evaluated following acid exposure). From earlier plots discussing the leaching of sodium, it was determined that a greater amount of sodium is leached in the first equilibrium set than in the second. In samples with a higher initial porosity, the acid may have penetrated further into the sample during the first exposure, resulting in a higher initial leaching of sodium.

In a previous study, the effectiveness of cation exchange materials in reducing the mobility of alkalis in the AAC material was examined. Vermiculite—a layered aluminosilicate mineral with Mg^{2+} and Fe^{2+} cations filling the void between layers—and Zeolite A were used as cation exchange materials, and their addition resulted in a reduction in sodium leachability [35]. However, in the present study, according to the response surfaces, sodium leaching was slightly increased by the addition of brucite. Thus, the differences in structures of the aluminosilicates, as well as the cation exchange material, can lead to differences in the response to acid exposure. In addition, the scatterplot in **Figure 22** shows a relationship between sodium and magnesium leaching. For high levels of sodium leaching, more magnesium appears to be retained and for low levels of sodium leaching, more magnesium is leached. This result was reflected in the response surfaces shown in **Section** Error! eference source not found. as well. This could indicate that with more sodium ions being leached out of the material, more magnesium ions from the dissolved brucite are being retained to replace them as charge-balancing ions in the aluminosilicate binder. This charge balance would stabilize the binder, preserving Si-O-Al bonds and reducing the amount of aluminum and silica leaching from the material.

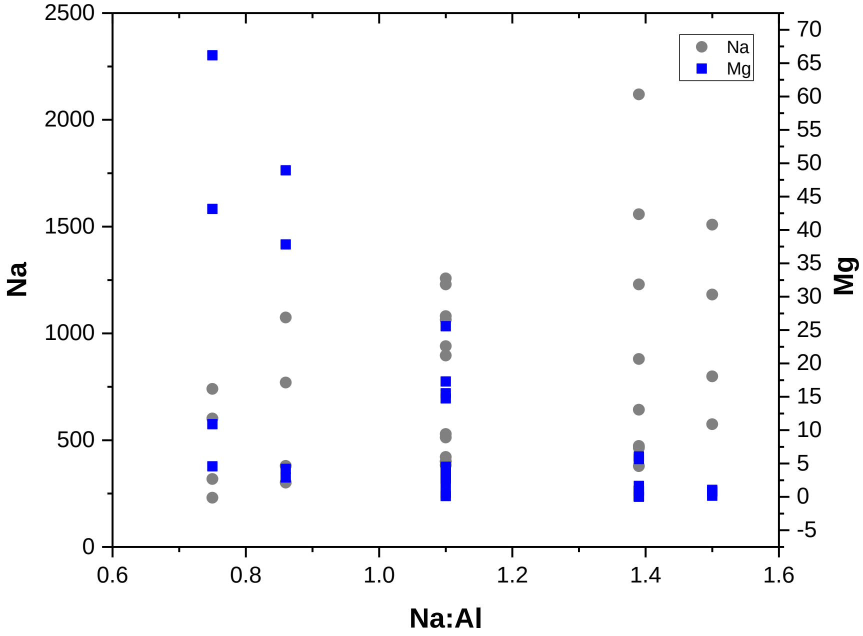

Figure 22. Scatterplot showing Na and Mg leaching concentration data (ppm) for different Na:Al ratios.

Even though porosity did not dictate leaching in this study, it is still an important characteristic to consider when evaluating the potential for the application of this type of material in an actual sewer environment. In this study, a stock sulfuric acid solution was prepared to test the material, but in the engineered system in which MICC occurs, the production of biogenic sulfuric acid is dependent on the concentrations of hydrogen sulfide, moisture, and oxygen present in the environment [35]. A reduction in porosity could reduce the availability of these components, decreasing the rate of the reaction producing biogenic sulfuric acid.

An additional consideration to take into account when evaluating real world application of this material is the effect of pH on the system. Sulfate-producing bacteria such as *Thiobacillus* cannot grow in conditions where they are directly exposed to high pH environments [35]. The pH of concrete made with OPC is ≈12. However, over time, carbonation at the surface of the concrete, in combination with hydrogen sulfide gas, results in a reduction in pH, creating an environment more conducive to sulfur oxidation and the growth of sulfate-producing bacteria [13]. In the equilibrium pH measurements taken after the material was exposed to acid, brucite-containing samples appeared to maintain a higher pH over multiple exposures. For most formulations, the equilibrium pH of the control sample solutions dropped dramatically between the first and second exposure, with 5 different mixture formulations reaching equilibrium at a $pH < 5.0$ in the second exposure. However, the equilibrium pH of the brucite addition samples remained high, with only one mixture formulation reaching equilibrium at a $pH < 5.0$ (in addition to the formulation that failed). The brucite addition appears to increase the capacity of the material to maintain a neutral pH which would be beneficial in an actual sewer environment where a higher pH could slow or stop the growth of sulfate-producing bacteria.

The addition of brucite to the metakaolin-based AAC formulations discussed appears to increase the overall acid resistance of the material by reducing the porosity of the material, maintaining a higher pH over multiple exposures, and reducing the leaching of silica and aluminum over multiple exposures. Both reduced porosity and a higher pH would create an environment less conducive to the growth of sulfate-producing bacteria in a real world setting while the reduction in the leaching of silica and aluminum indicates a more intact aluminosilicate binder, implying greater acid resistance.

CHAPTER 6 CONCLUSION

6.1 SUMMARY

The aim of this study was to systematically evaluate the role of magnesium on the acid resistance of metakaolin-based AACs by introducing brucite, a magnesium mineral, and measuring bulk permeable porosity, elemental leaching, mineralogy, and changes in composition following acid exposure.

The results from this work establish that the addition of brucite to a calcium-free, metakaolin-based AAC improves its overall acid resistance. Several factors contributing to this improvement in acid resistance included: reduced porosity, a reduction of dependency on alkali content for apparent stability within the aluminosilicate framework, and consequently, a reduction in the amount of silicon and aluminum leached from the AACs containing brucite. The addition of brucite led to a reduced initial porosity and final porosity after acid exposure compared to the experimental controls. While the results show that porosity did not solely act as a covariate with the amount of silicon and aluminum leached, it is an important material bulk physical property to note as it could affect the performance of the material in an actual sewer environment in which sulfate-producing bacteria are present.

Another key finding of this study concerns the diminished importance of silica and alkali content on maintaining low porosity during acid exposure when magnesium is present in the system. The data substantiate that the change in porosity during acid exposure in the samples with a brucite addition is not as dependent on alkali content as the control samples. The interaction between alkali content and silica content is also less important in determining the change in porosity during acid exposure in AACs containing brucite than the experimental controls.

One of the most useful findings in understanding the improved acid resistance of the AACs with a brucite addition is the reduction in leached aluminum and silicon over multiple exposures in comparison with the control AACs. This reduction confirms that the stability of the aluminosilicate framework is improved with the magnesium mineral addition likely through a cation-exchange mechanism involving magnesium and elemental sodium.

Finally, both experiments and statistical modeling of data elucidate that the most acid-resistance sample formulations included those with Na:Si ratios ≈ 0.75 with high amounts of both sodium and silica. This conclusion was determined from the silica and aluminum leaching response surfaces, porosity response surfaces, and the electron microprobe analysis data that, together, showed that samples that best met these criteria experienced minimal dealumination.

6.2 LIMITATIONS OF THE STUDY

One of the limitations of this study is the variance between in the water to binder ratio (and water to solids ratio) between the control and brucite samples due to the large Mg:Si ratio explored and the resulting added mass of the brucite. A smaller amount or a varying Mg:Si ratio would have been more beneficial to the study, allowing for a more useful comparison of the porosity between the control and brucite-containing samples. Varying the Mg:Si ratio would also allow for the development of response surfaces that would provide further information on the optimal Mg:Si ratio and would allow the study to focus more directly on the effect of magnesium on the acid resistance of metakaolin-based AACs rather than evaluating the effects of varying alkali and silicate concentrations.

An additional limitation of this study is the method employed to evaluate permeable porosity. The vacuum ethanol intrusion methodology for measuring porosity is overly destructive to the samples, potentially leading to higher values of porosity than reflect reality.

6.3 RECOMMENDATIONS FOR FUTURE WORK

Future studies testing the application of AACs would benefit from creating a more realistic sewer environment to test the results presented, especially those related to porosity and pH. Creating this type of environment could yield a better understanding of how a brucite addition to metakaolin-based AACs could potentially inhibit the growth of sulfate-producing bacteria and prevent the cause of MICC.

In addition, in this study, the control and brucite-containing samples were only exposed to fresh acid solutions and allowed to reach equilibrium twice. In order to determine how much of a lasting effect the brucite addition has on the pH of the acid solution once equilibrium has been reached, it would be beneficial to increase the number of exposures or to evaluate the time-dependent leaching behavior of the samples.

Another aspect of this study that would benefit from further examination is the effect of mineralogy on the acid resistance of AACs. In this study, two mixture formulations resulted in the formation of minerals – in one case Zeolite A was formed and in the other case Faujasite-Na was formed. Focusing on a smaller subset of mixture formulations that would be likely to result in the formation of one or more of these minerals could be valuable for evaluating the effect of mineralogy on the properties of the material and its significance in determining the overall acid resistance of the material.

As mentioned earlier in this work, one of the key benefits of AACs is the ability to manipulate their properties to design for certain conditions. Further study regarding the use of cation exchange materials in AACs is needed in order to more fully understand how they can be used to manipulate the properties of the material.

REFERENCES

[1] ASCE, “2017 Infrastructure Report Card: Wastewater,” 2017.

[2] C. B. Office, “Future Investment in Drinking Water and Wastewater Infrastructure,” 2002.

[3] US EPA, “Clean Watersheds Needs Survey 2012,” *United States Environ. Prot. Agency*, vol. 53, no. 9, pp. 1689–1699, 2012.

[4] A. P. Joseph, J. Keller, H. Bustamante, and P. L. Bond, “Surface neutralization and H2S oxidation at early stages of sewer corrosion: Influence of temperature, relative humidity and H2S concentration,” *Water Res.*, vol. 46, no. 13, pp. 4235–4245, 2012.

[5] A. L. Ling *et al.*, “Carbon dioxide and hydrogen sulfide associations with regional bacterial diversity patterns in microbially induced concrete corrosion,” *Environ. Sci. Technol.*, vol. 48, no. 13, pp. 7357–7364, 2014.

[6] A. Allahverdi and F. Skvara, “Acidic corrosion of hydrated cement based materials. Part 1. Mechanism of the Phenomenon,” *Ceramics-Silikáty*, vol. 44, no. 4, pp. 152–160, 2000.

[7] T. Mori, M. K. Y. Hikosaka, T. Nonaka, F. M. Y. Sakai, and J. Koizumi, “MICROBIAL CORROSION OF CONCRETE SEWER PIPES , H2S PRODUCTION FROM SEDIMENTS AND DETERMINATION OF CORROSION RATE,” *Water Sci. Technol.*, vol. 23, pp. 1275–1282, 1991.

[8] T. Bakharev, J. G. Sanjayan, and Y. B. Cheng, “Resistance of alkali-activated slag concrete to acid attack,” *Cem. Concr. Res.*, vol. 33, no. 10, pp. 1607–1611, 2003.

[9] F. Pacheco-Torgal, J. Castro-Gomes, and S. Jalali, “Alkali-activated binders: A review. Part 1. Historical background, terminology, reaction mechanisms and hydration products,” *Constr. Build. Mater.*, vol. 22, no. 7, pp. 1305–1314, 2008.

[10] L. K. Turner and F. G. Collins, “Carbon dioxide equivalent (CO 2 -e) emissions : A comparison between geopolymer and OPC cement concrete,” *Constr. Build. Mater.*, vol. 43, pp. 125–130, 2013.

[11] I. Garcia-Lodeiro, A. Palomo, and A. Fernández-Jiménez, *An overview of the chemistry of alkali-activated cement-based binders*. Woodhead Publishing Limited, 2014.

[12] A. Kumar *et al.*, “The Atomic-Level Structure of Cementitious Calcium Silicate Hydrate,” *J. Phys. Chem. C*, vol. 121, no. 32, pp. 17188–17196, 2017.

[13] J. L. Provis, A. Fernández-jiménez, E. Kamseu, C. Leonelli, and A. Palomo, *Alkali Activated Materials*, vol. 13. 2014.

[14] S. A. Bernal *et al.*, *Alkali Activated Materials*, vol. 13. 2014.

[15] J. L. Provis, A. Palomo, and C. Shi, “Cement and Concrete Research Advances in understanding alkali-activated materials,” *Cem. Concr. Res.*, vol. 78, pp. 110–125, 2015.

[16] J. L. Provis, P. Duxson, J. S. J. van Deventer, and G. C. Lukey, “The role of

mathematical modelling and gel chemistry in advancing geopolymer technology," *Chem. Eng. Res. Des.*, vol. 83, no. 7 A, pp. 853–860, 2005.

[17] A. Allahverdi and Š. Frantisek, "SULFURIC ACID ATTACK ON HARDENED PASTE OF GEOPOLYMER CEMENTS PART 1 . MECHANISM OF CORROSION AT RELATIVELY HIGH CONCENTRATIONS," *Ceramics*, pp. 225–229, 2005.

[18] C. Li, H. Sun, and L. Li, "A review: The comparison between alkali-activated slag (Si + Ca) and metakaolin (Si + Al) cements," *Cem. Concr. Res.*, vol. 40, no. 9, pp. 1341–1349, 2010.

[19] S. J. O'Connor, K. J. D. MacKenzie, M. E. Smith, and J. V. Hanna, "Ion exchange in the charge-balancing sites of aluminosilicate inorganic polymers," *J. Mater. Chem.*, vol. 20, pp. 10234–10240, 2010.

[20] J. Davidovits, "PROPERTIES OF GEOPOLYMER CEMENTS Joseph Davidovits Geopolymer Institute, Cordi-Geopolymère SA, 16 rue Galilée, 02100 Saint-Quentin, France," *Geopolymer Inst.*, pp. 1–19, 1994.

[21] C. Shi and J. A. Stegemann, "Acid corrosion resistance of different cementing materials," vol. 30, pp. 0–5, 2000.

[22] T. Bakharev, "Resistance of geopolymer materials to acid attack," *Cem. Concr. Res.*, vol. 35, no. 4, pp. 658–670, 2005.

[23] C. Grengg, F. Mittermayr, N. Ukrainczyk, G. Koraimann, S. Kienesberger, and M. Dietzel, "Advances in concrete materials for sewer systems affected by microbial induced concrete corrosion: A review," *Water Res.*, vol. 134, pp. 341–352, 2018.

[24] P. Sturm, G. J. G. Gluth, C. Jäger, H. J. H. Brouwers, and H. Kühne, "Sulfuric acid resistance of one-part alkali-activated mortars," *Cem. Concr. Res.*, vol. 109, no. April, pp. 54–63, 2018.

[25] M. A. M. Ariffin, M. A. R. Bhutta, M. W. Hussin, M. M. Tahir, and N. Aziah, "Sulfuric acid resistance of blended ash geopolymer concrete," vol. 43, pp. 80–86, 2013.

[26] R. R. Lloyd, J. L. Provis, and J. S. J. Van Deventer, "Acid resistance of inorganic polymer binders. 1. Corrosion rate," *Mater. Struct. Constr.*, vol. 45, no. 1–2, pp. 1–14, 2012.

[27] J. P. Gevaudan, K. M. Campbell, T. J. Kane, R. K. Shoemaker, and W. V. Srubar, "Mineralization dynamics of metakaolin-based alkali-activated cements," *Cem. Concr. Res.*, vol. 94, pp. 1–12, 2017.

[28] X. Huang, S. Hu, F. Wang, Y. Liu, and Y. Mu, "Properties of alkali-activated slag with addition of cation exchange material," *Constr. Build. Mater.*, vol. 146, pp. 321–328, 2017.

[29] B. Walkley, R. San Nicolas, and S. Bernal, "Effect of MgO incorporation on the structure of synthetic alkali-activated calcium aluminosilicate binders," *Conf. 27th Bienn. Natl. Conf. Concr. Inst. Aust.*, no. August 2015, 2015.

[30] A. Palomo, *Crucial insights on the mix design of alkali-activated cement-based binders*. Woodhead Publishing Limited, 2015.

[31] D. R. M. Brew and F. P. Glasser, "Synthesis and characterisation of

magnesium silicate hydrate gels," *Cem. Concr. Res.*, vol. 35, no. 1, pp. 85–98, 2005.

[32] D. Nied, K. Enemark-rasmussen, E. L. Hopital, J. Skibsted, and B. Lothenbach, "Properties of magnesium silicate hydrates (M-S-H)," *Cem. Concr. Res.*, vol. 79, pp. 323–332, 2016.

[33] A. Allahverdi and Š. Frantisek, "SULFURIC ACID ATTACK ON HARDENED PASTE OF GEOPOLYMER CEMENTS PART 2 . CORROSION MECHANISM AT MILD AND RELATIVELY LOW CONCENTRATIONS," *Ceramics*, pp. 3–6, 2005.

[34] F. Pacheco-Torgal, Z. Abdollahnejad, A. F. Camões, M. Jamshidi, and Y. Ding, "Durability of alkali-activated binders: A clear advantage over Portland cement or an unproven issue?," *Constr. Build. Mater.*, vol. 30, pp. 400–405, 2012.

[35] T. Mori, T. Nonaka, K. Tazaki, M. Koga, Y. Hikosaka, and S. Noda, "INTERACTIONS OF NUTRIENTS , MOISTURE AND pH ON MICROBIAL CORROSION OF CONCRETE SEWER PIPES," *Water Res.*, vol. 26, no. I, pp. 29–37, 1991.

APPENDIX

7.1 Additional XRD plots

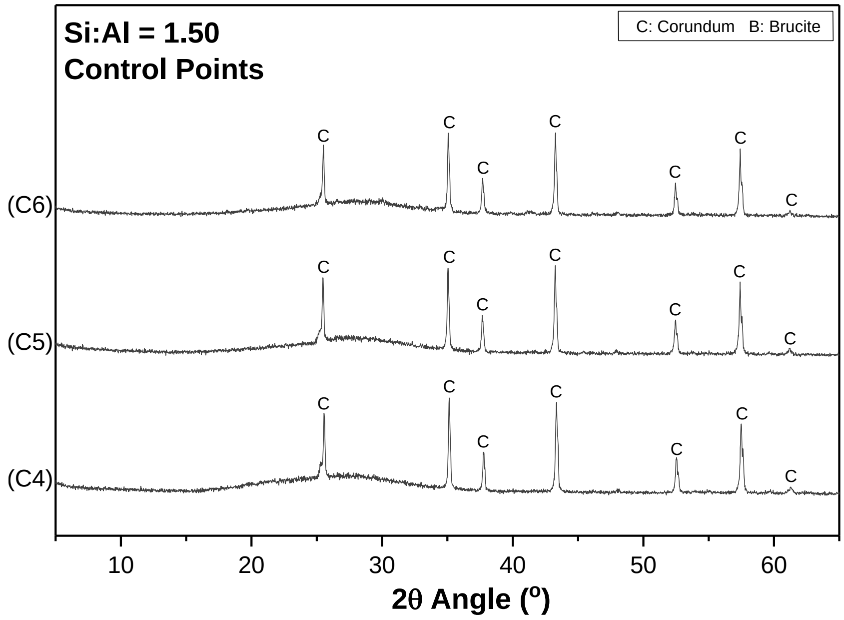

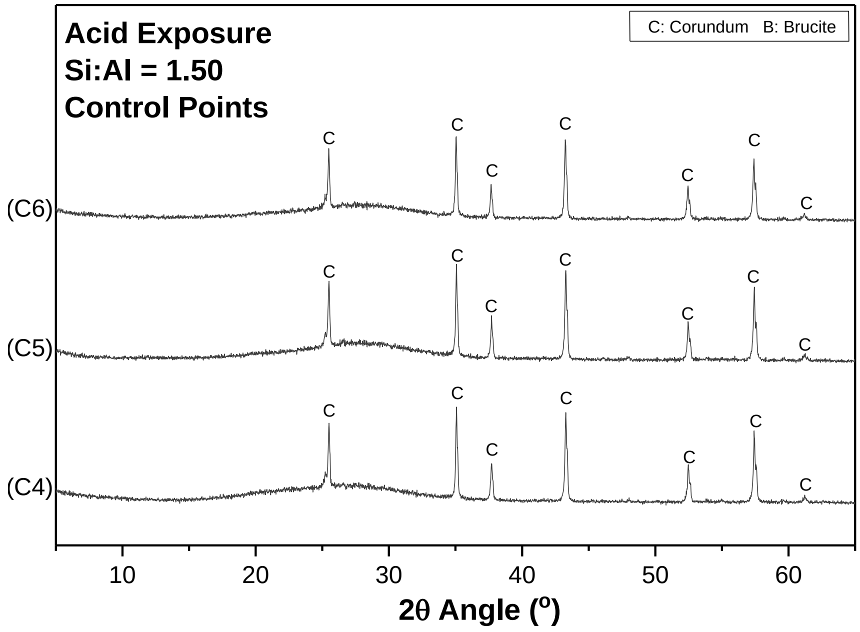

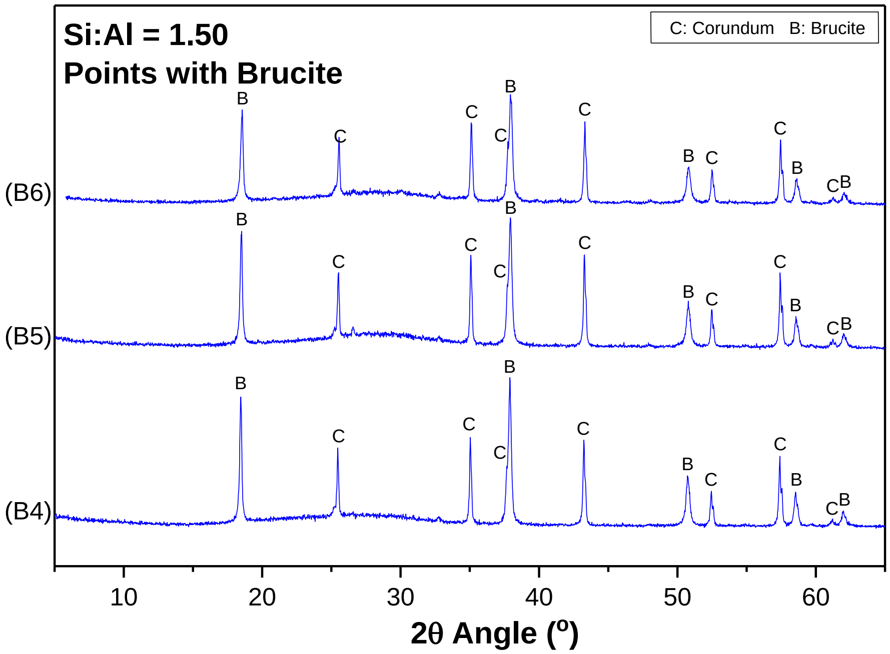
Si:Al = 1.50
Points with Brucite
C: Corundum B: Brucite
(B6)
(B5)
(B4)
B
C
C
C
B
C
B
C
C
B
C B
10
20
30
40
50
60
2θ Angle (º)

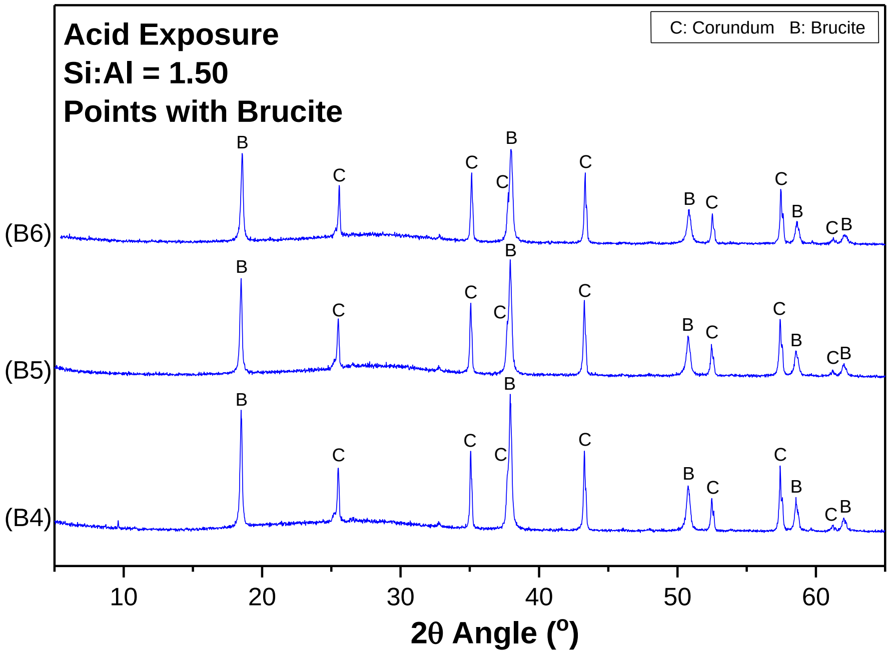
Acid Exposure
Si:Al = 1.50
Points with Brucite
C: Corundum B: Brucite
(B6)
(B5)
(B4)
B
C
C
C
B
C
B
C
C
B
C B
10
20
30
40
50
60
2θ Angle (º)

7.2 Elemental map color intensity scales

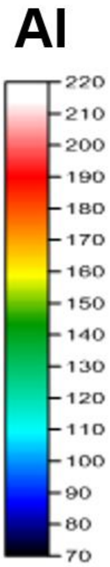

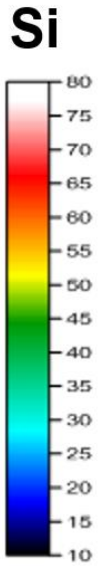

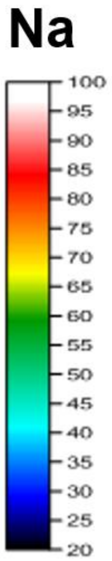

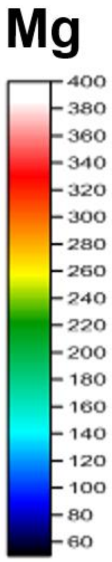

7.3 Normality plots and residuals and fits graphs for the leaching response surfaces.

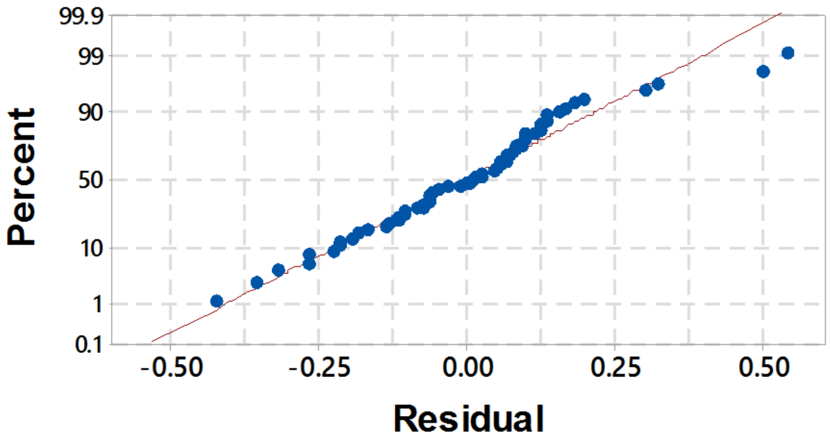

Figure 23. Sodium leaching residuals normality plot indicates a normal distribution after the Box-Cox data transformation.

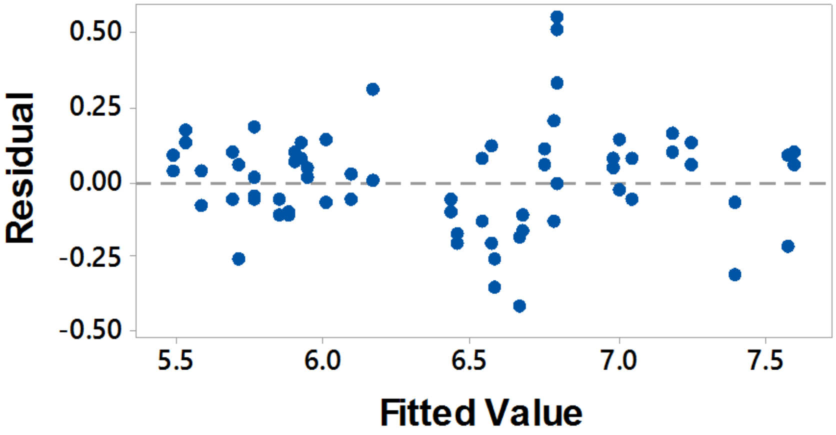

Figure 24. Residuals and fits graph for the model describing sodium leaching.

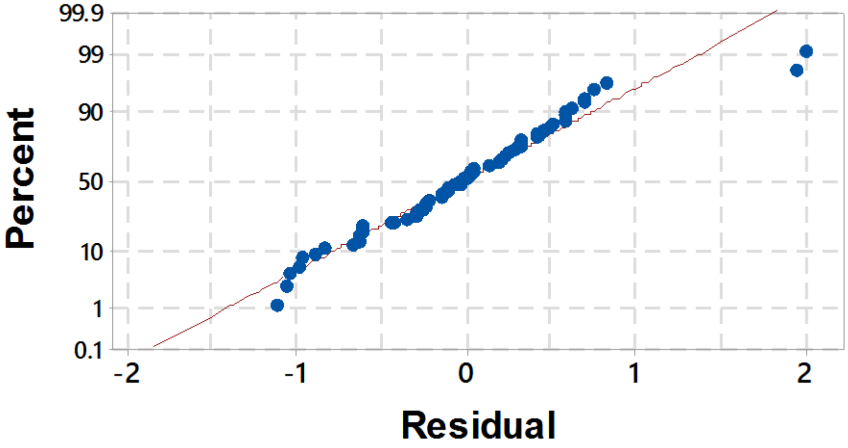

Figure 25. Silicon leaching residuals normality plot indicates a normal distribution after the Box-Cox data transformation.

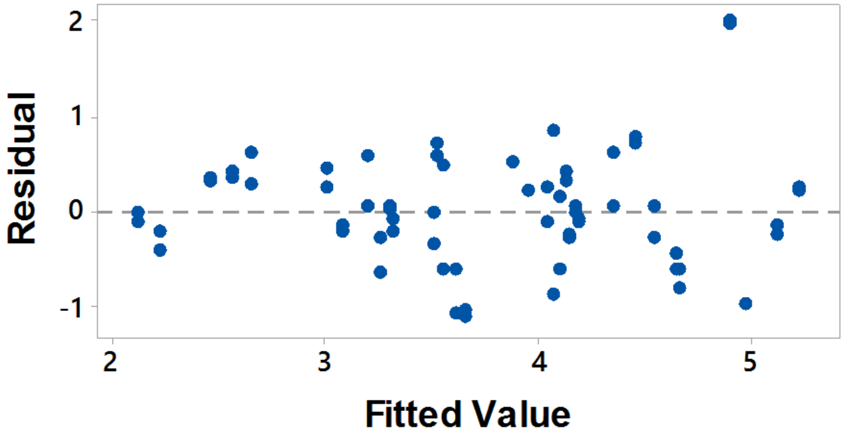

Figure 26. Residuals and fits for the model describing silicon leaching.

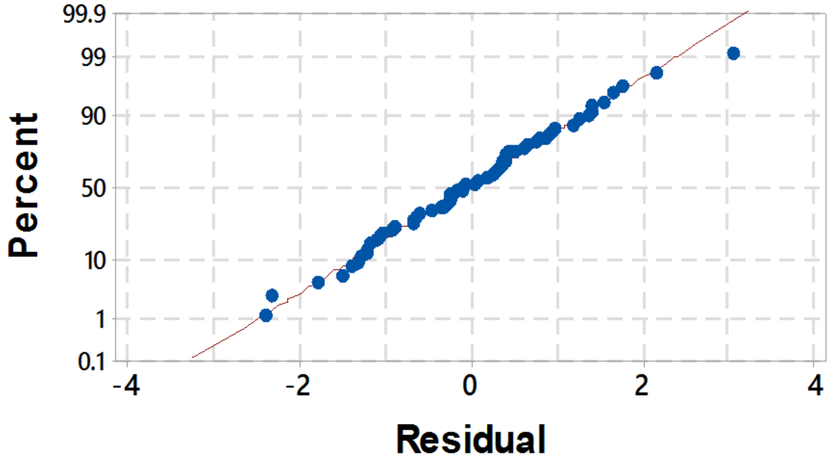

Figure 27. Aluminum residuals normality plot indicates a normal distribution after the Box-Cox data transformation.

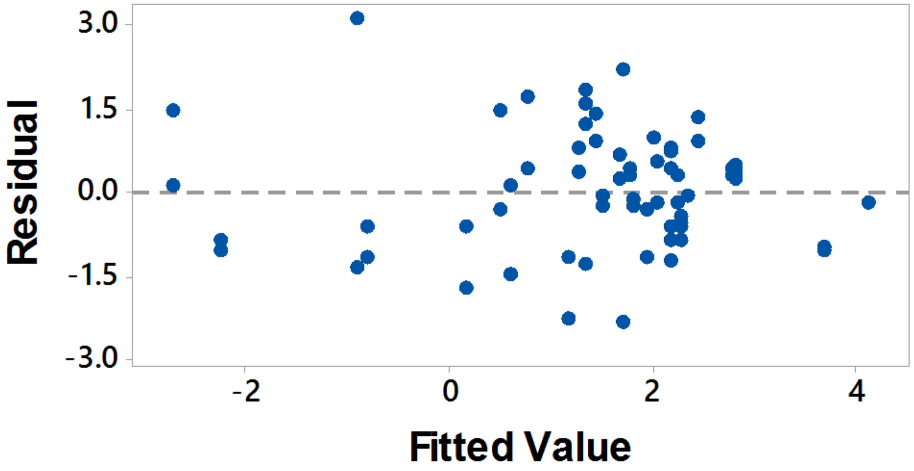

Figure 28. Residuals and fits for the model describing aluminum leaching.

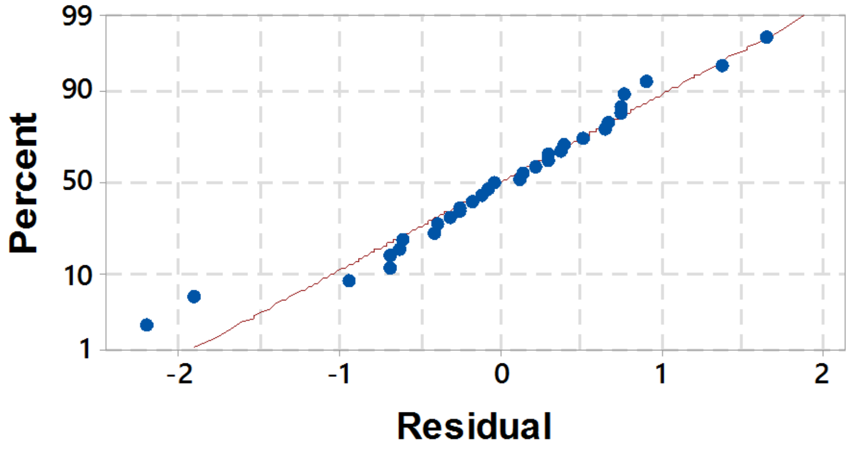

Figure 29. Magnesium Residuals normality plot indicates a normal distribution after the Box-Cox data transformation.

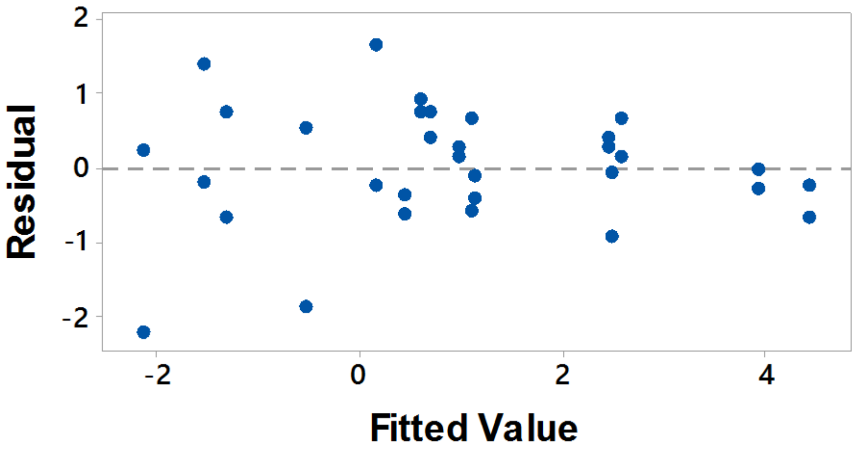

Figure 30. Residuals and fits for the model describing magnesium leaching.